Electronic Supplementary Material (ESI) for Photochemical & Photobiological Science

Supporting Information

Highly Photostable "Super"-Photoacids for Ultrasensitive Fluorescence Spectroscopy

Björn Finkler[a], Christian Spies[a], Michael Vester[a], Frederick Walte[a], Kathrin Omlor[a], Iris Riemann[b], Manuel Zimmer[c], Frank Stracke[b], Markus Gerhards[c], Gregor Jung[a]

[a] Biophysical Chemistry, Saarland University, Campus B2 2, 66123 Saarbrücken, Germany.

[b] Fraunhofer-IBMT, Ensheimer Straße 48, 66386 St. Ingbert, Germany.

[c] Technische Universität Kaiserslautern & Research Center Optimas, Fachbereich Chemie, Erwin-Schrödinger-Str.
67663 Kaiserslautern, Germany.

Email corresponding author: g.jung@mx.uni-saarland.de

Determination of pK_a values via fluorescence correlation spectroscopy (FCS)

For determination of the pK_a values of the weakly water soluble photoacids, we followed the experimental procedure of Widegren *et al.* [S1]

The actual system consists of an acid, the corresponding base and buffer HB^+/B for stabilizing the equilibrium. A 20 mM HPCE-buffer (citric acid / sodium citrate, Fluka) was employed for the pH values 4 and 4.5. Protonation and deprotonation is widely mediated by HB^+ and B with the bimolecular rate constants k_{prot}^{bi} and k_{deprot}^{bi} (Equation S1), which are experimentally determined to lie in the range of ~ $10^8\ \mathrm{M^{-1}s^{-1}}$. At a total buffer concentration of 20 mM, where $[\mathrm{HB^+}] \approx [\mathrm{B}]$, direct, diffusion-controlled protonation by H^+ and deprotonation can be neglected at pH-values > 4.[S1]

$$\mathrm{ROH + B} \underset{\mathrm{k}_{prot}^{bi}}{\overset{\mathrm{k}_{deprot}^{bi}}{\rightleftharpoons}} \mathrm{RO^- + HB^+} \qquad \text{(S1)}$$

The kinetic description for the equilibrium leads to:

$$\frac{d[\mathrm{RO^-}]}{dt} = -\mathrm{k}_{prot}^{bi}[\mathrm{RO^-}][\mathrm{HB^+}] + \mathrm{k}_{deprot}^{bi}[\mathrm{ROH}][\mathrm{B}] = 0 \qquad \text{(S2)}$$

The effective rates are defined as $\mathrm{k}_{prot}^{eff} = \mathrm{k}_{prot}^{bi} \cdot [\mathrm{HB^+}]$ and $\mathrm{k}_{deprot}^{eff} = \mathrm{k}_{deprot}^{bi} \cdot [\mathrm{B}]$, so equation S2 can be converted into:

$$\frac{[\mathrm{ROH}]}{[\mathrm{RO^-}]} = \frac{\mathrm{k}_{prot}^{eff}}{\mathrm{k}_{deprot}^{eff}} \qquad \text{(S3)}$$

$$K_a^{-1} = \frac{[\mathrm{ROH}]}{[\mathrm{H^+}][\mathrm{RO^-}]} \qquad \text{(S4)}$$

Combination of (S3) and (S4) leads to a relation for the pK_a:

$$\mathrm{p}K_a = \mathrm{pH} + log\,\frac{\mathrm{k}_{prot}^{eff}}{\mathrm{k}_{deprot}^{eff}} \qquad \text{(S5)}$$

The rate constants k_{prot}^{eff} and $\mathrm{k}_{deprot}^{eff}$ are directly accessible in a FCS-experiment by photoexcitation of RO^- and detection of its fluorescence (Figure S1).

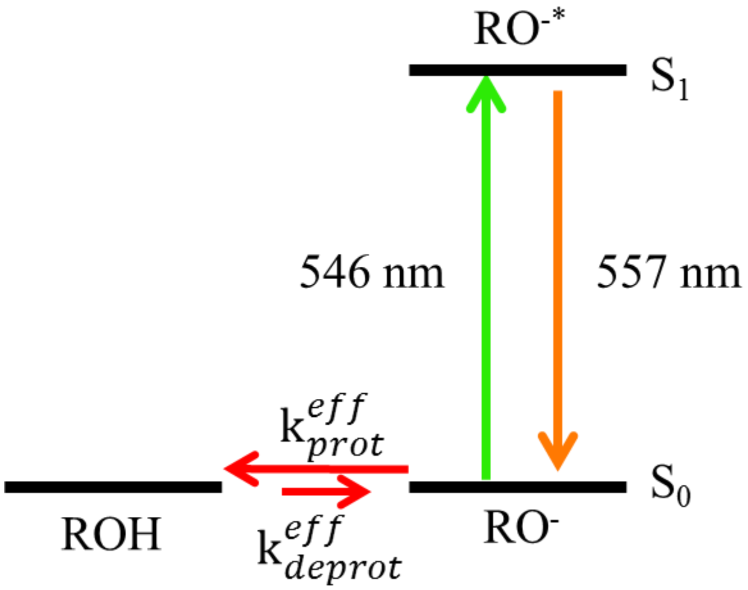

Figure S1: Schematic representation for pK_a-determination: excitation of RO$^-$ (**3b**) was performed at λ_{exc} = 546 nm ($\lambda_{abs,\,max}$ = 515 nm at pH 4; $\lambda_{em,\,max}$ = 557 nm at pH 4), fluorescence was detected at λ_{det} = 555-625 nm. The dark state ROH is populated with the rate constant k_{prot}^{eff}, whereas k_{deprot}^{eff} describes the depopulation the dark state.

Fitting the obtained correlation functions G(τ) according to equation S6 (Figure S2) gives the rates k_{prot}^{eff}, k_{deprot}^{eff} and consequently the pK_a value depicted in Table 2. The outcome of this approach was verified with **3f**.

$$G(\tau) = \frac{1}{\langle N \rangle} \frac{1}{1+\frac{\tau}{\tau_D}} \left(1 + \frac{k_{prot}^{eff}}{k_{deprot}^{eff}} \exp\left(-(k_{prot}^{eff} + k_{deprot}^{eff})\tau\right) \right) \qquad \text{(S6)}$$

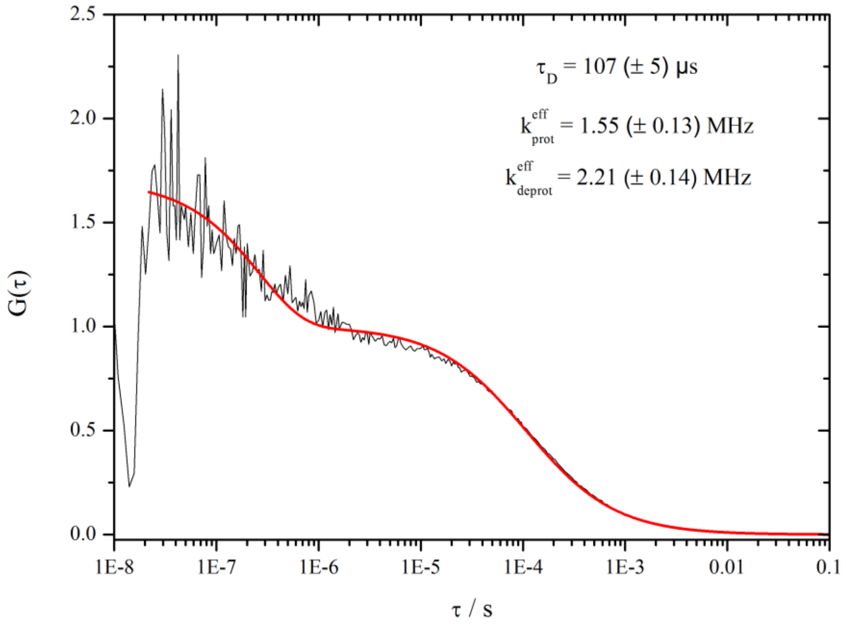

Figure S2: Normalized correlation function of **3b**. Excitation was performed at λ = 546 nm with a laser intensity of 168 kW cm^{-1} in a 20 mM citrate-buffer at pH 4.5. Fluorescence was detected at λ_{det} = 555-625 nm. A pK_a of 4.4 is calculated as a mean value of two measurements.

Characterisation of the described compounds with NMR- and mass spectroscopy:

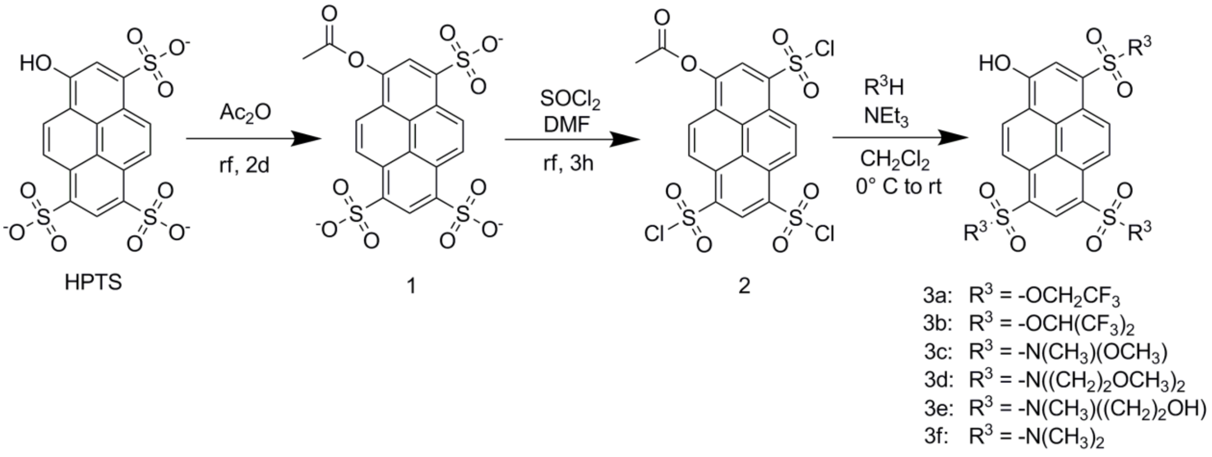

Scheme S1: Synthesis of HPTS-derivatives **3a**-**f**.

Compound **1**:

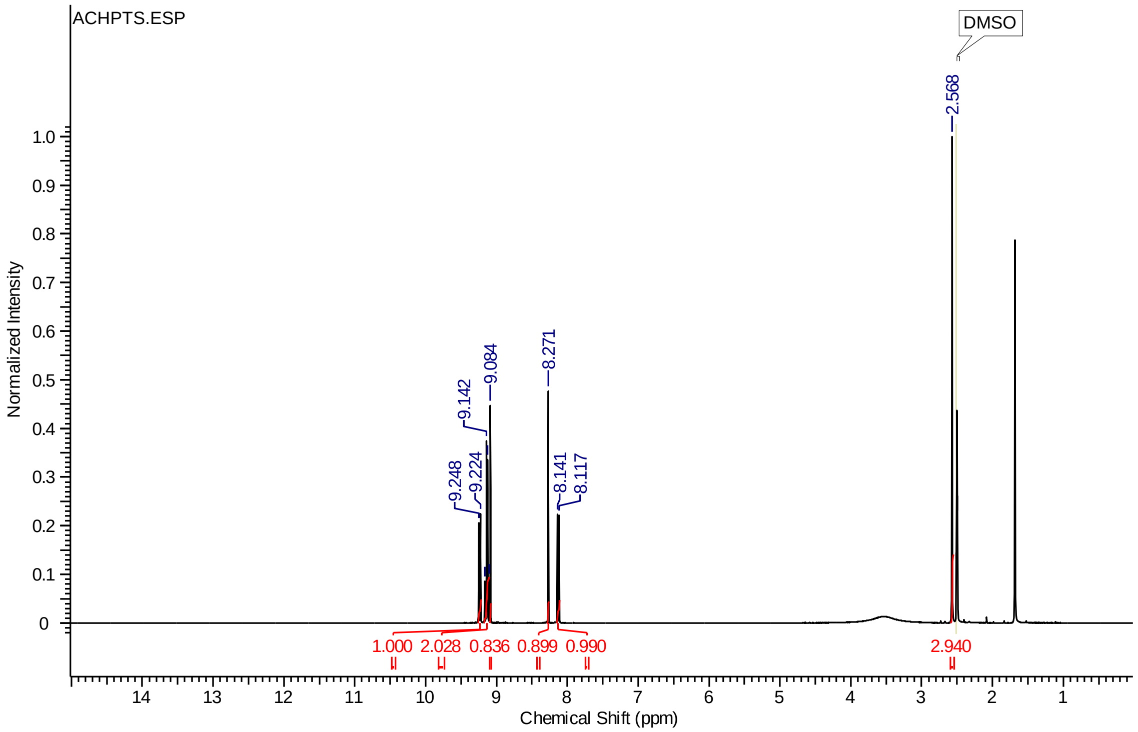

Figure S3: ^{1}H-NMR spectrum of **1**.

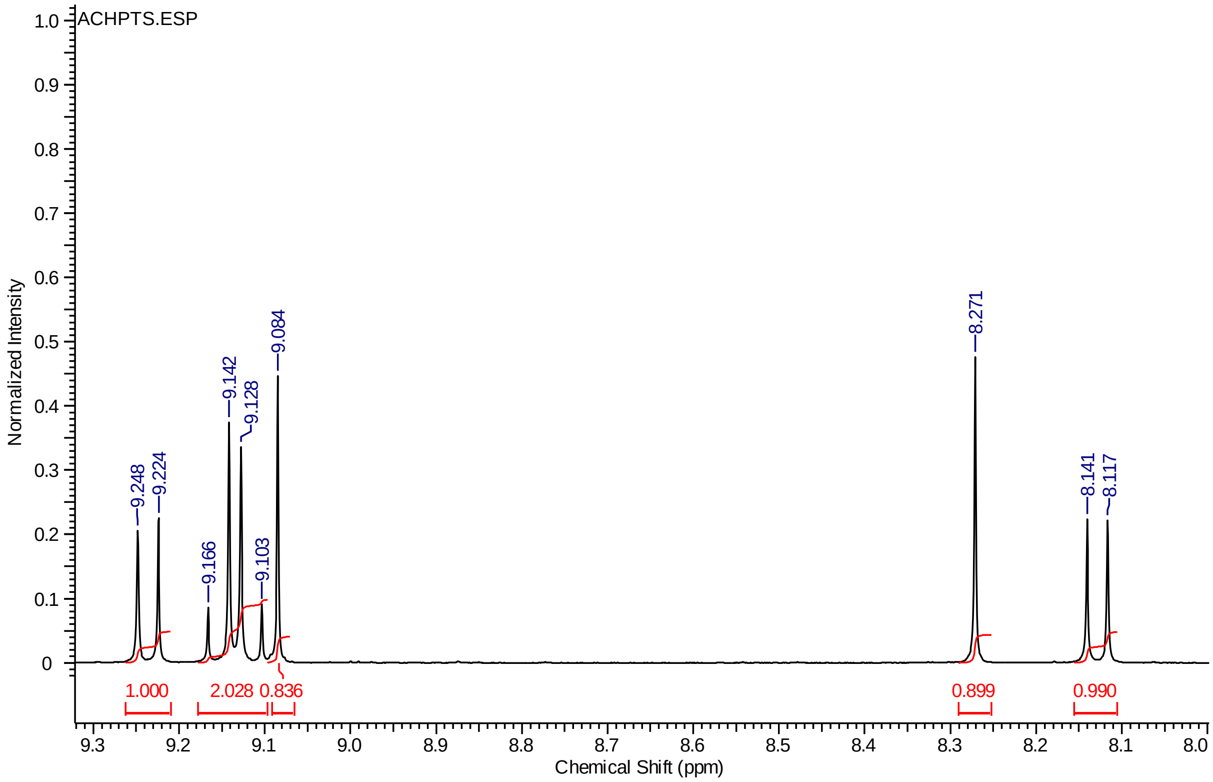

Figure S4: ^{1}H-NMR spectrum of **1** (zoomed).

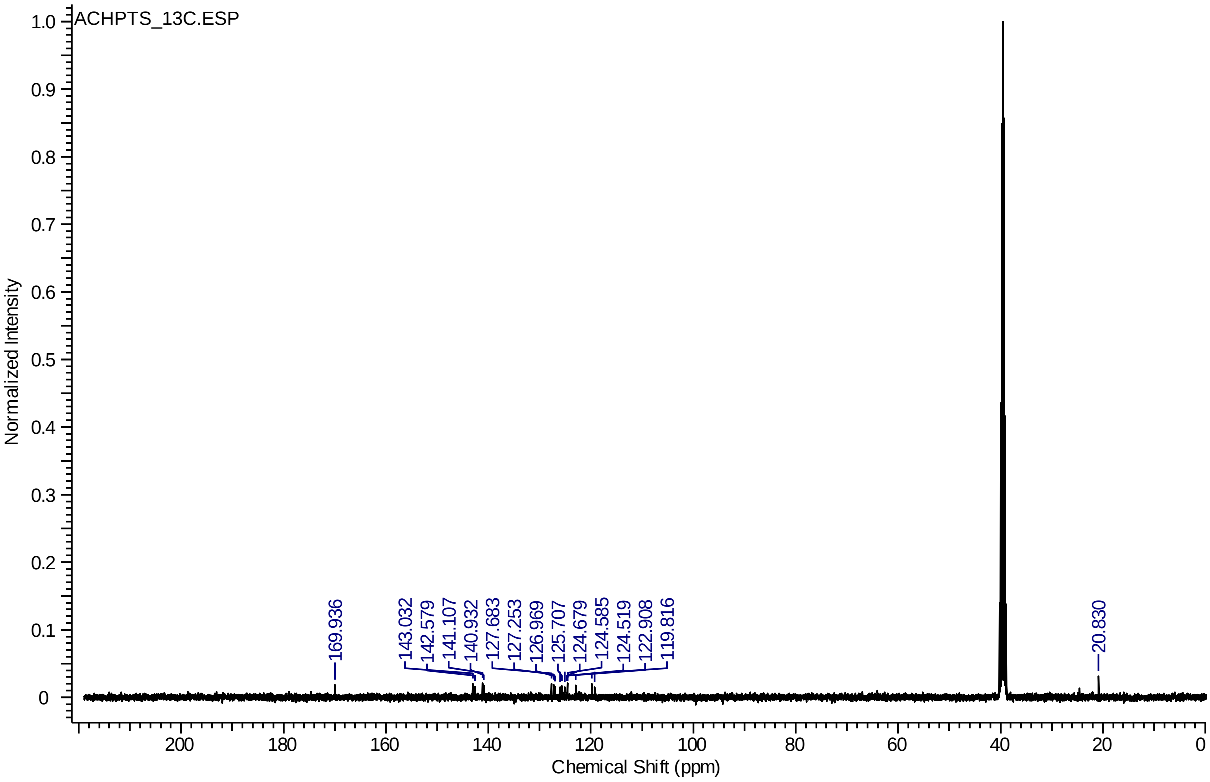

Figure S5: ^{13}C-NMR spectrum of **1**.

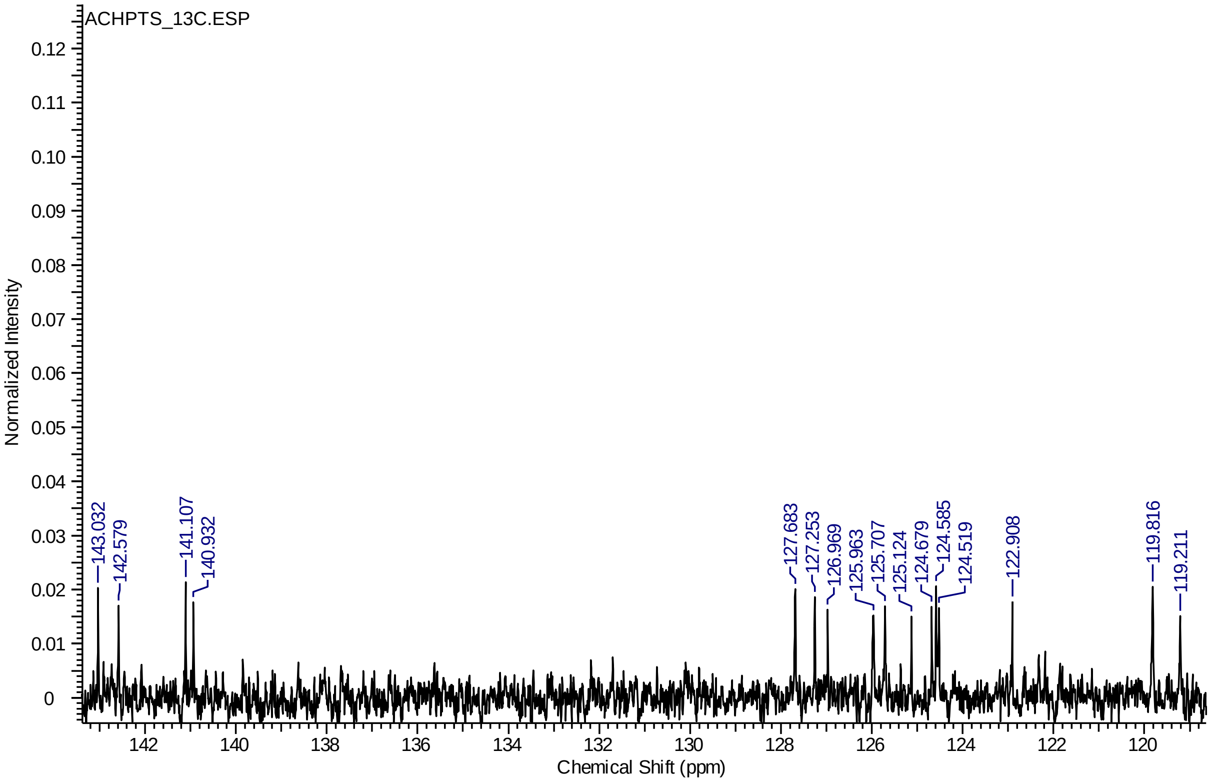

Figure S6: ^{13}C-NMR spectrum of **1** (zoomed).

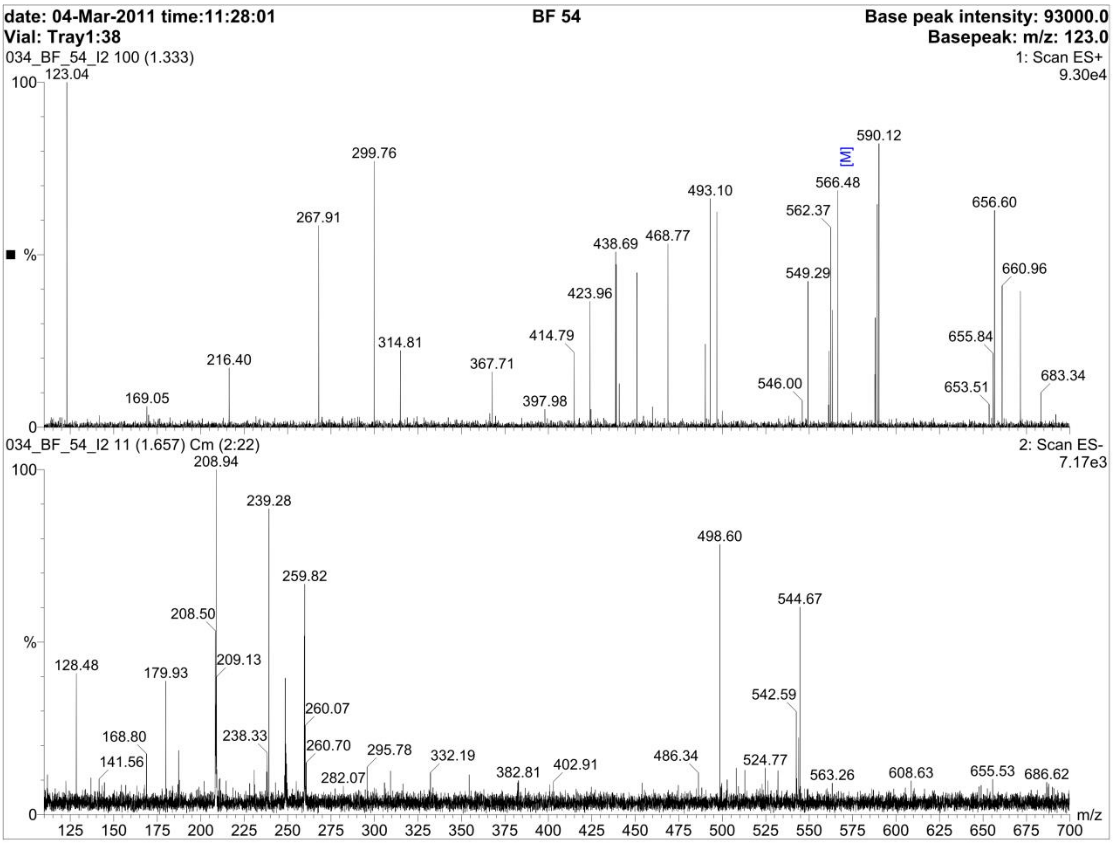

Figure S7: mass spectrum of **1**.

Compound **2**:

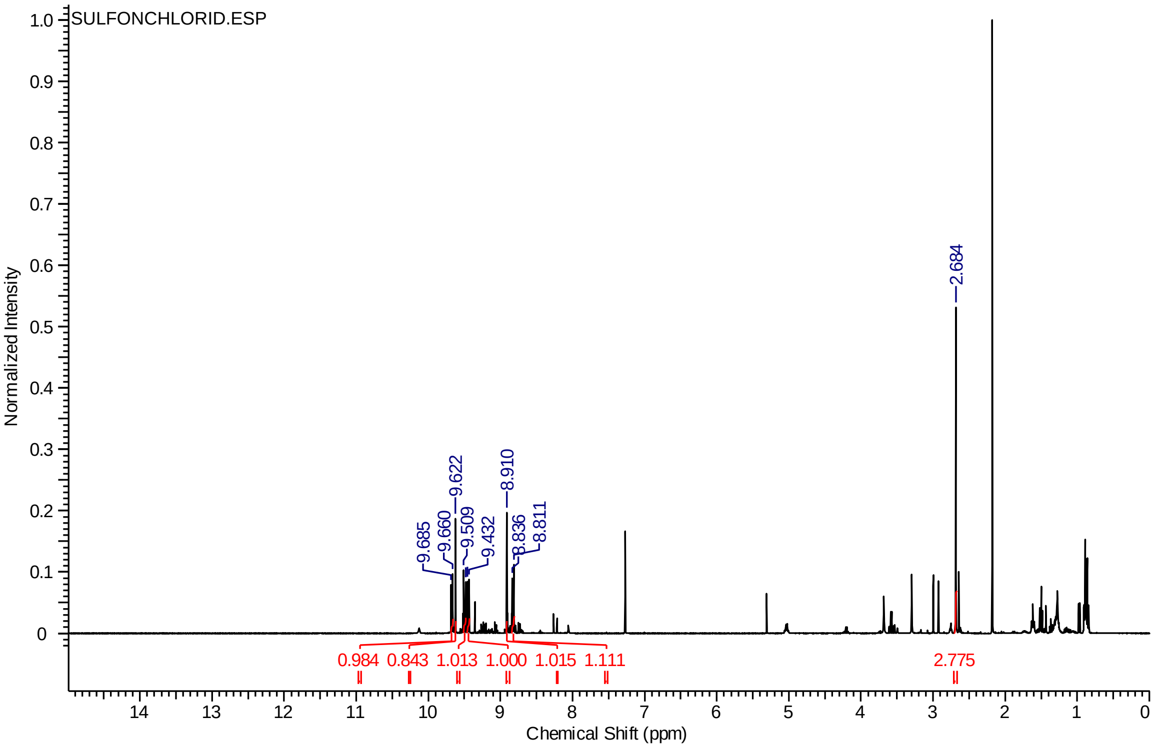

Figure S8: ^{1}H-NMR spectrum of **2**.

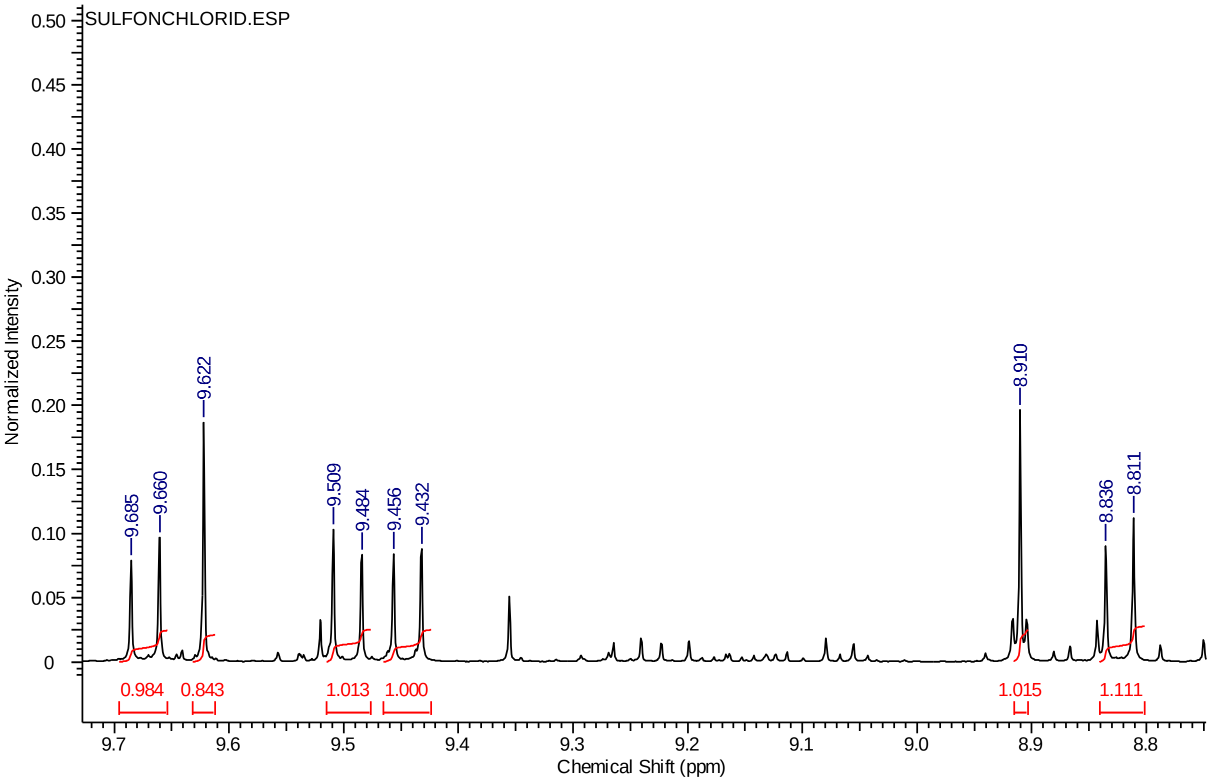

Figure S9: ^{1}H-NMR spectrum of **2** (zoomed).

Compound **3a**:

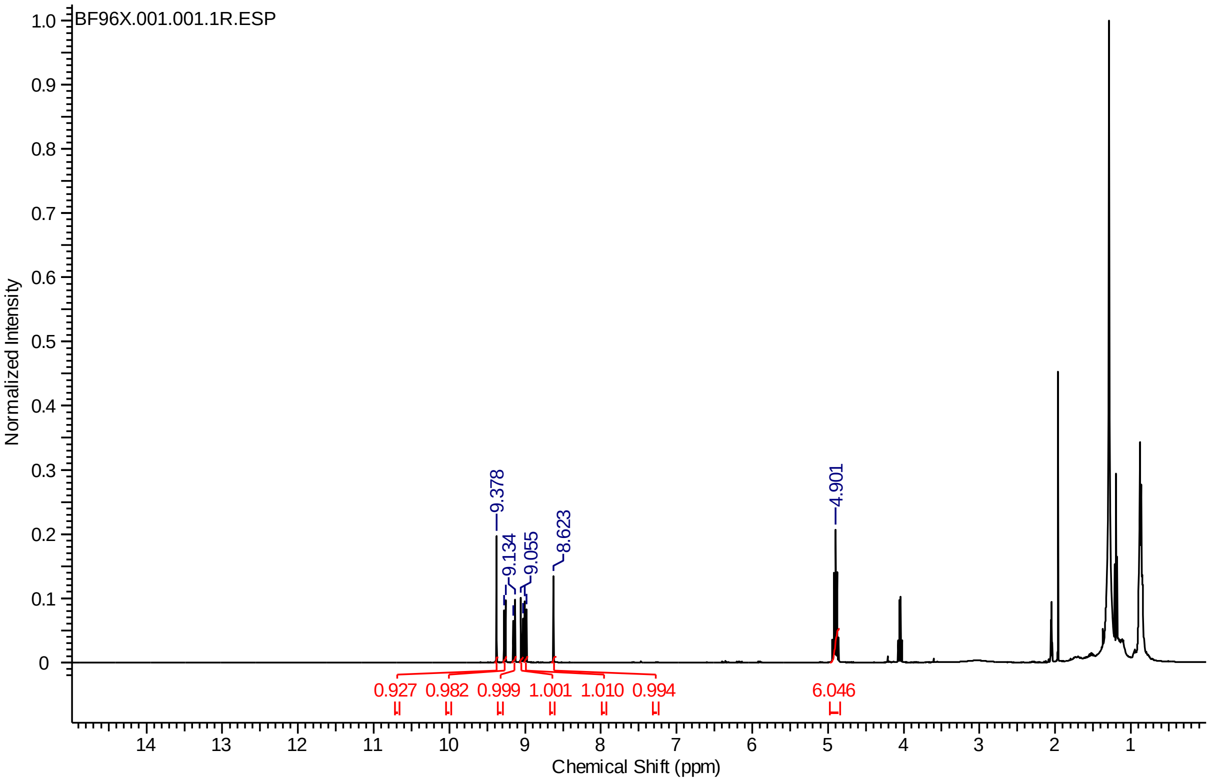

Figure S10: ^{1}H-NMR spectrum of **3a**.

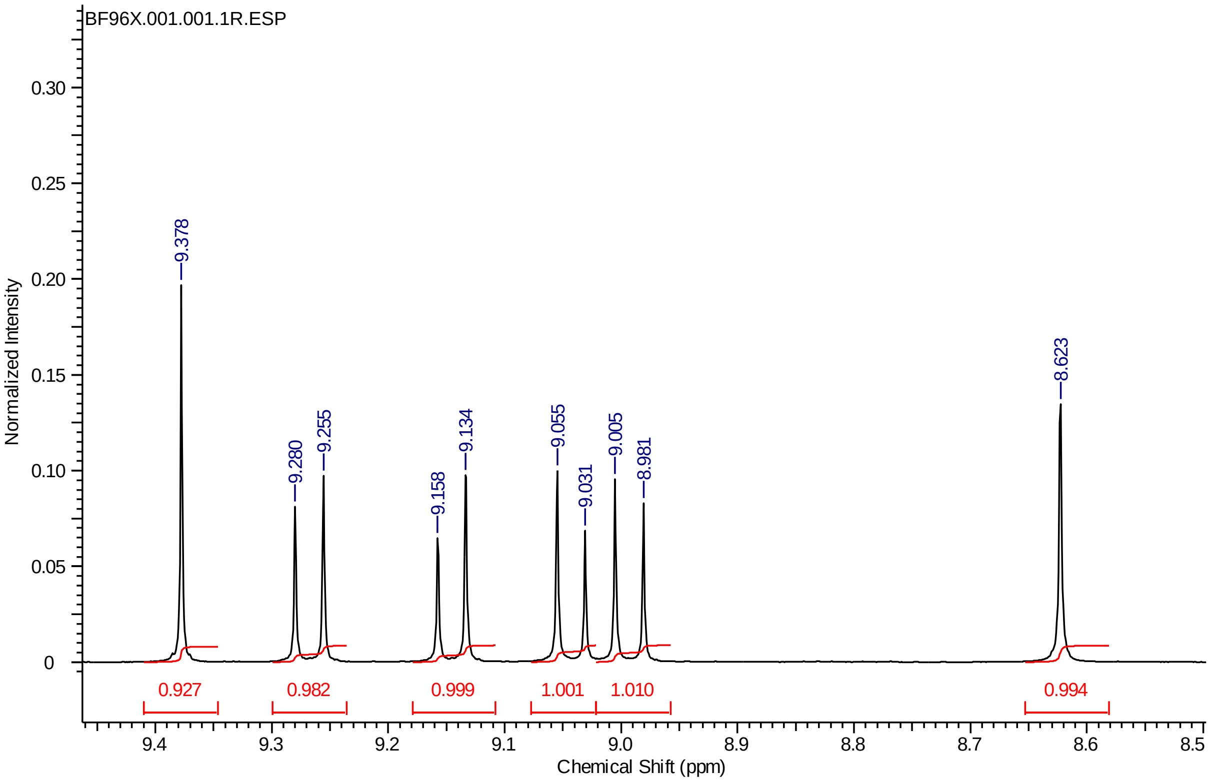

Figure S11: ^{1}H-NMR spectrum of **3a** (zoomed).

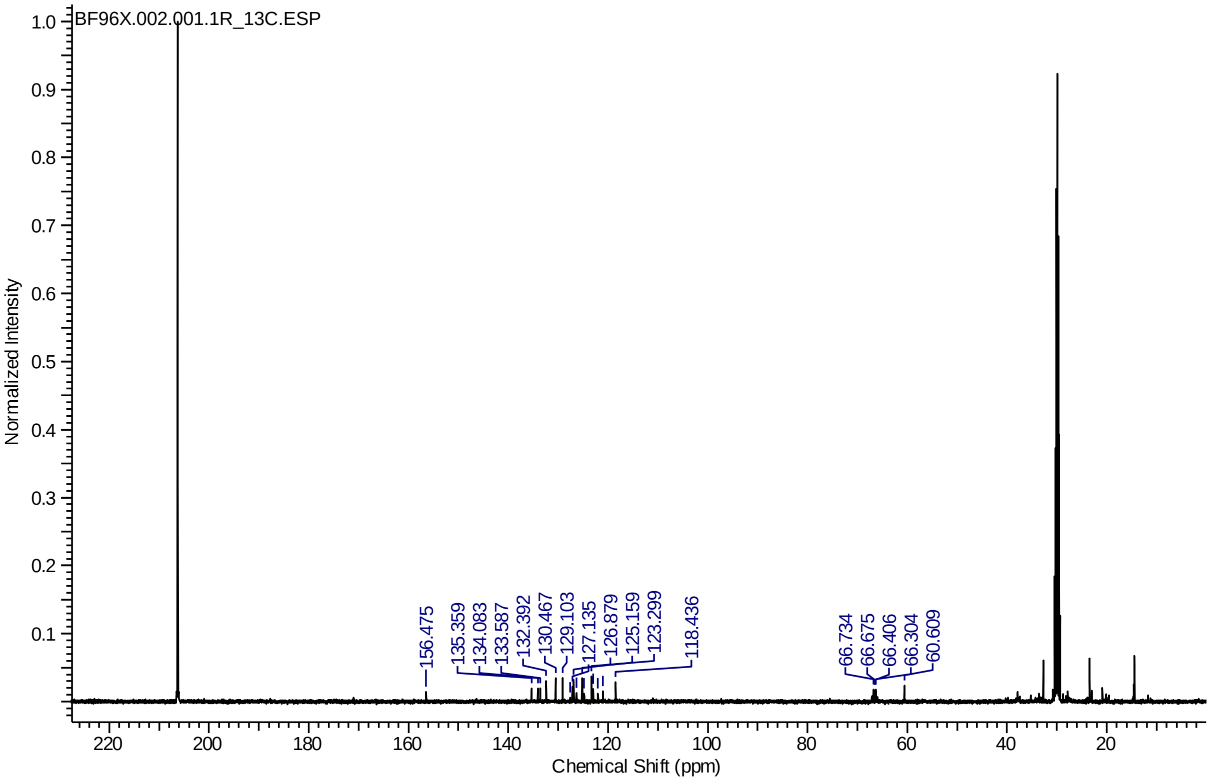

Figure S12: ^{13}C-NMR spectrum of **3a**.

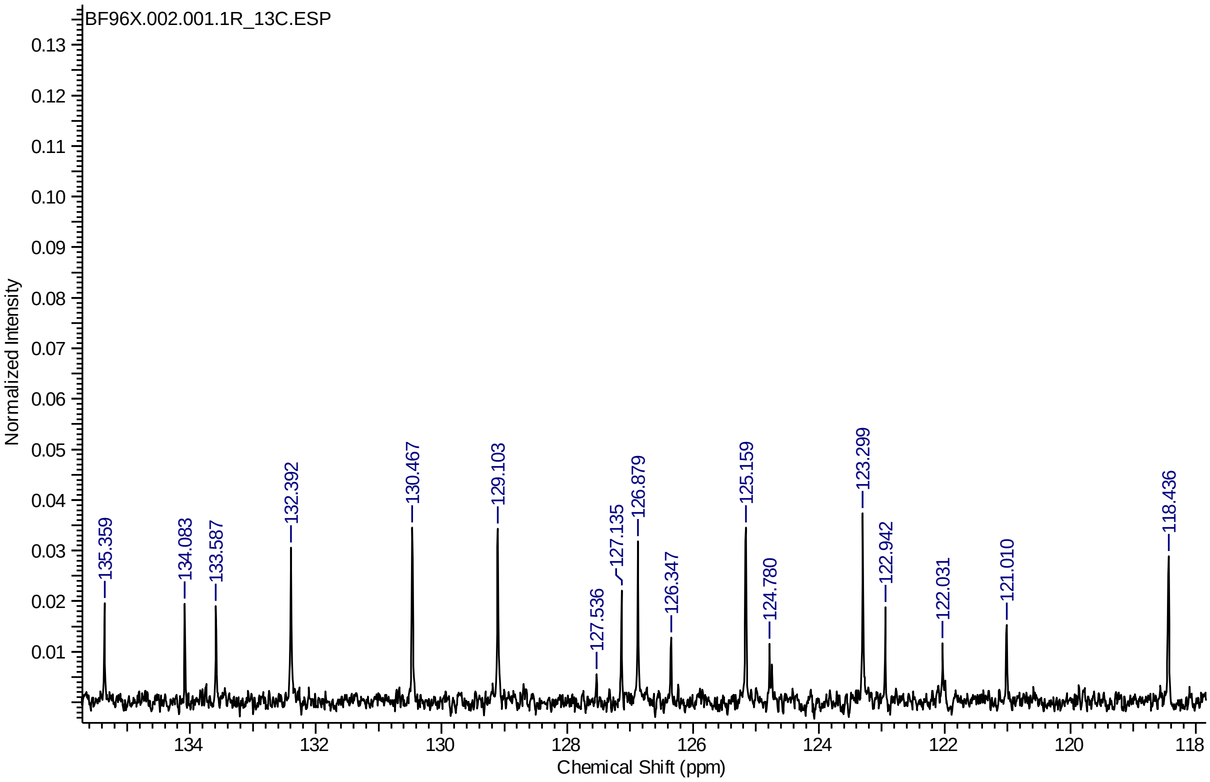

Figure S13: ^{13}C-NMR spectrum of **3a** (zoomed).

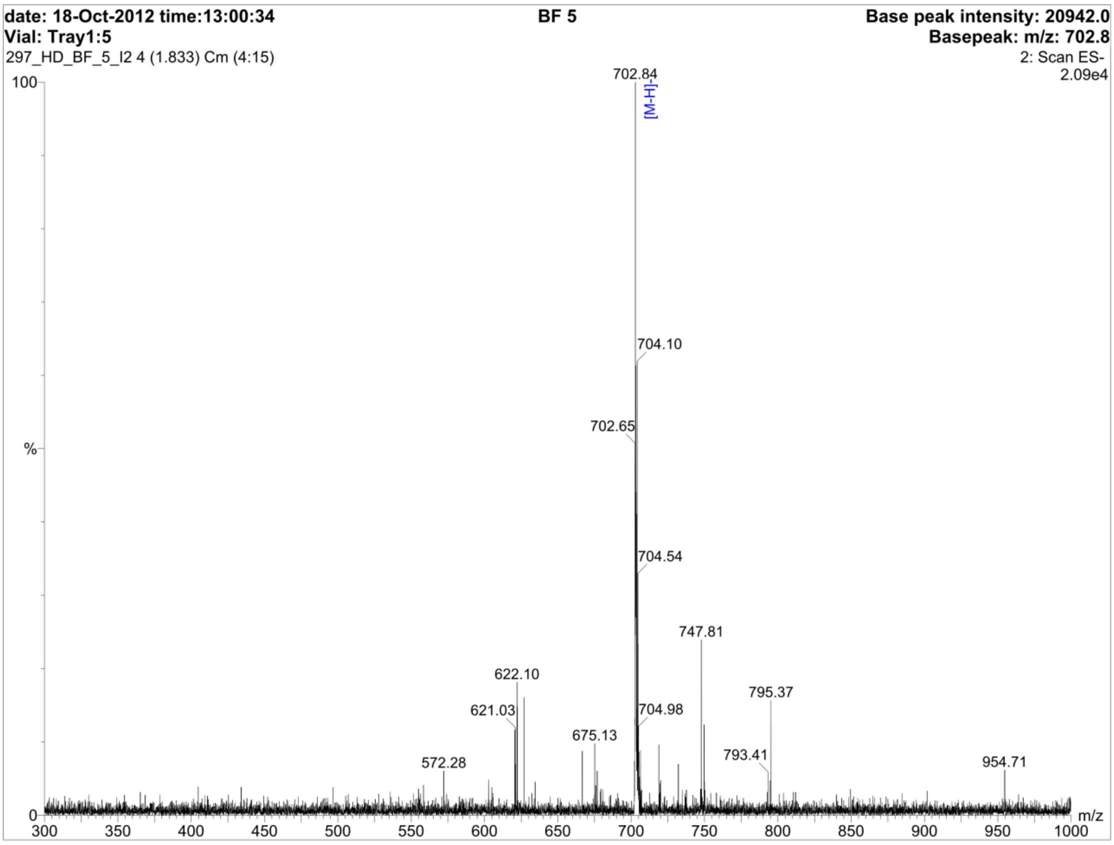

Figure S14: mass spectrum of **3a**.

Compound **3b**:

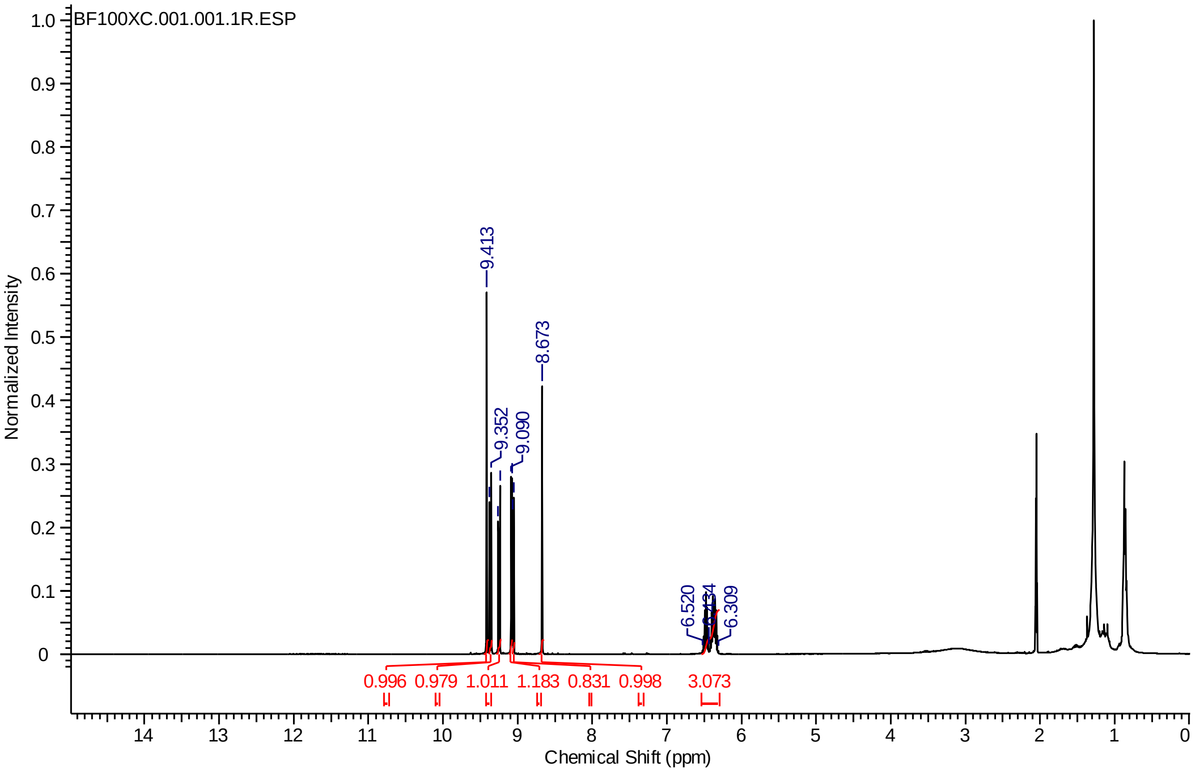

Figure S15: ^{1}H-NMR spectrum of **3b**.

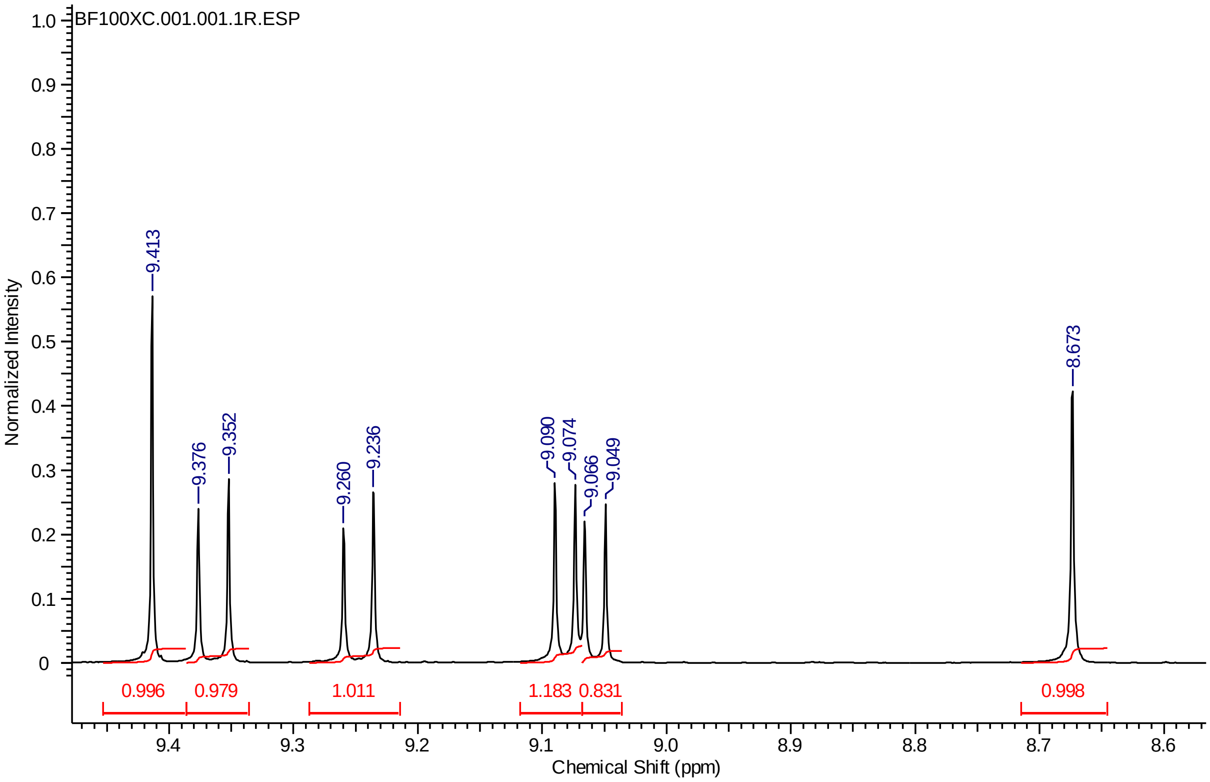

Figure S16: ^{1}H-NMR spectrum of **3b** (zoomed).

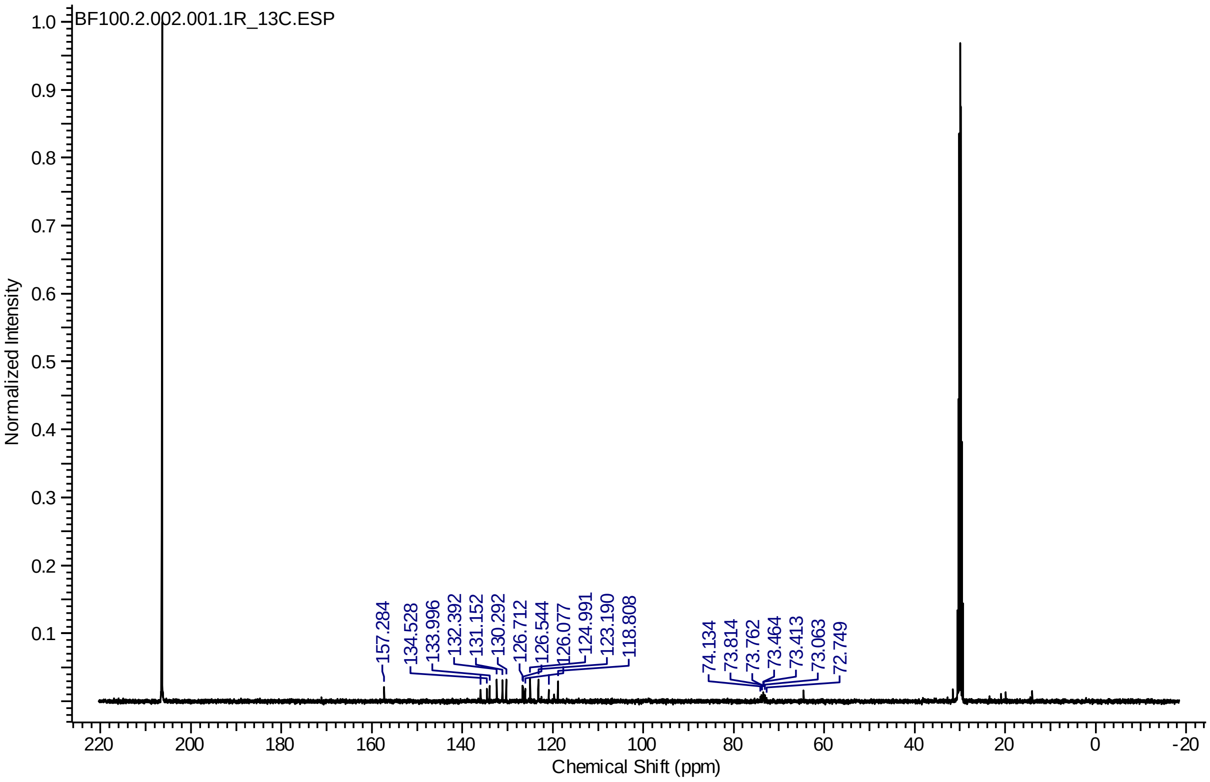

Figure S17: ^{13}C-NMR spectrum of **3b**.

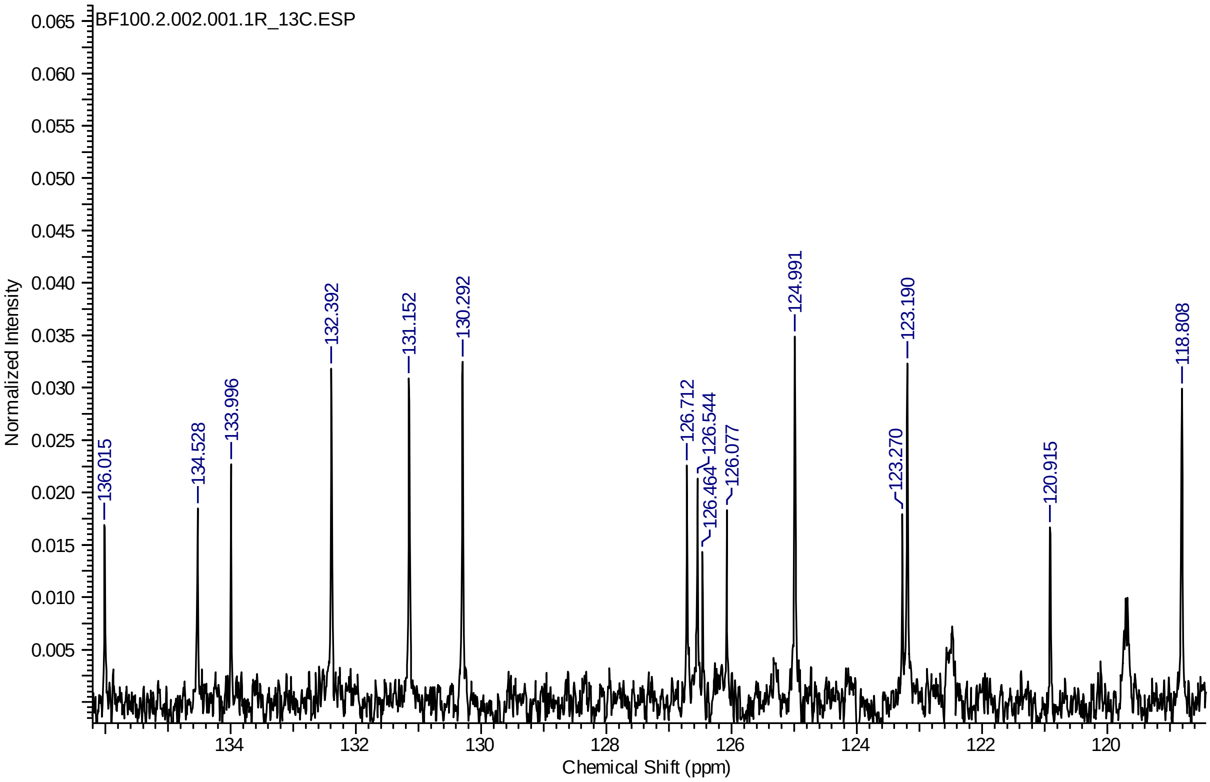

Figure S18: ^{13}C-NMR spectrum of **3b** (zoomed).

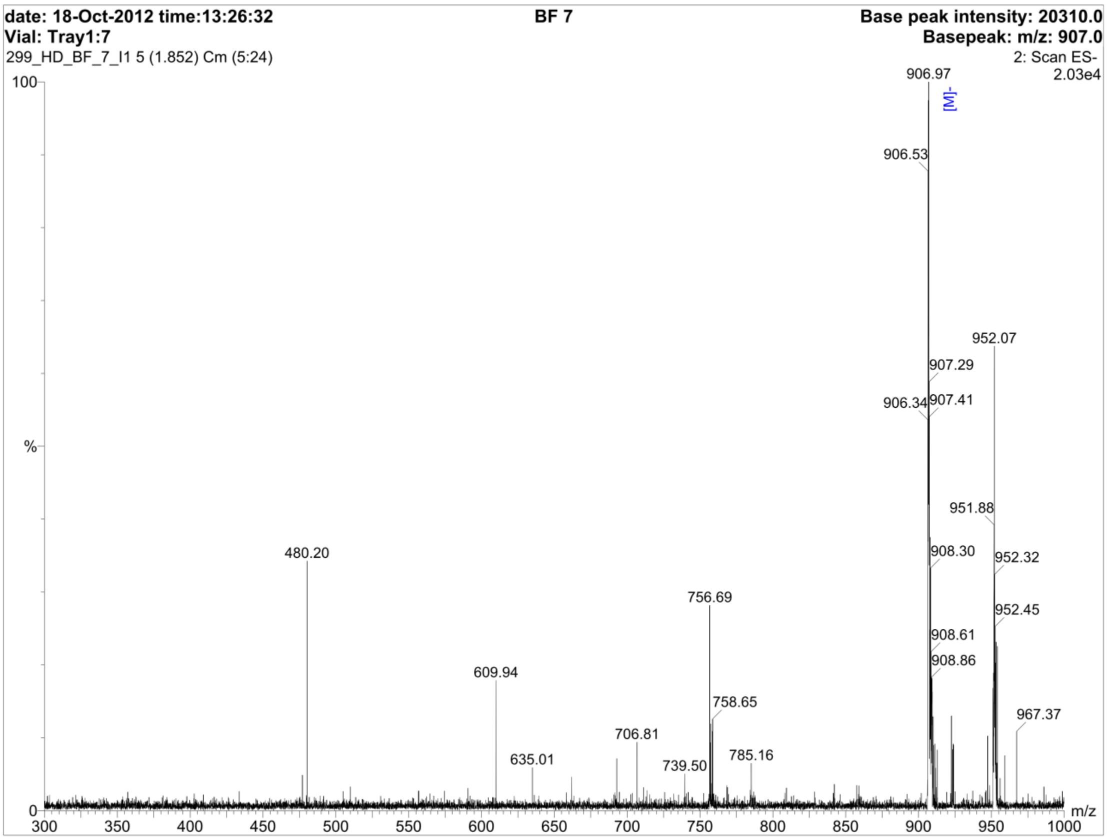

Figure S19: mass spectrum of **3b**.

Compound **3c**:

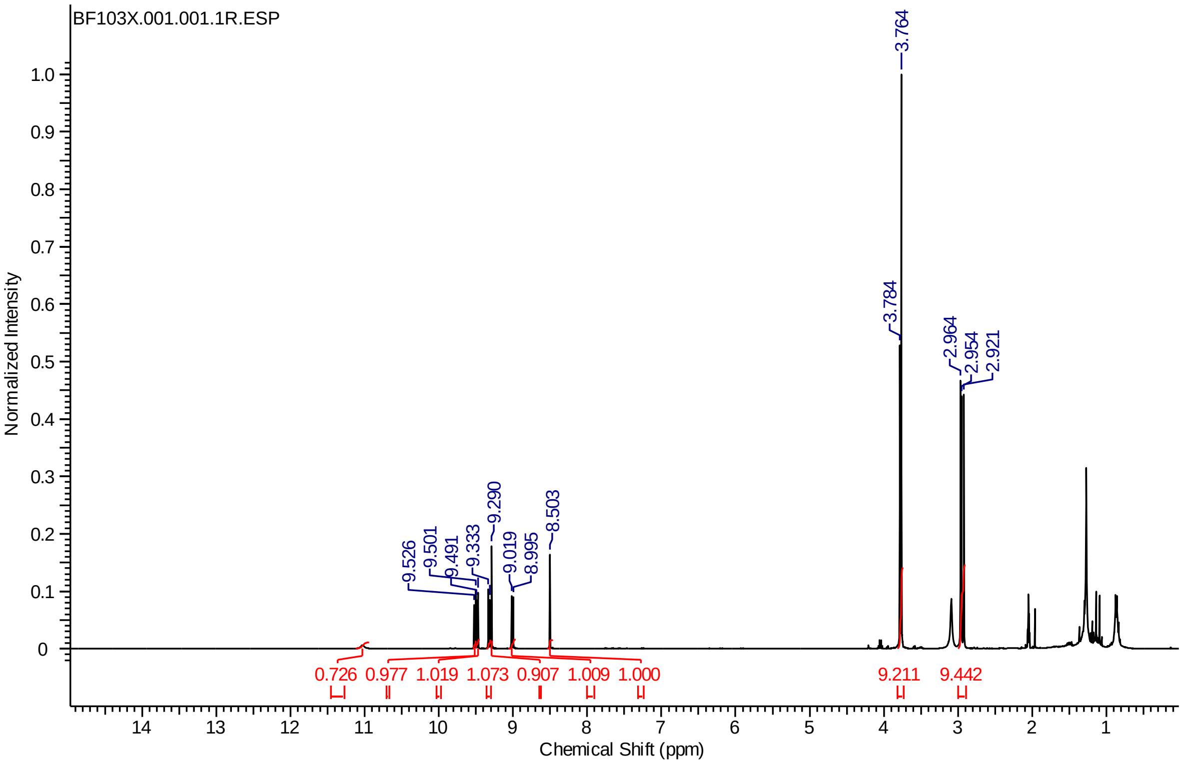

Figure S20: ^{1}H-NMR spectrum of **3c**.

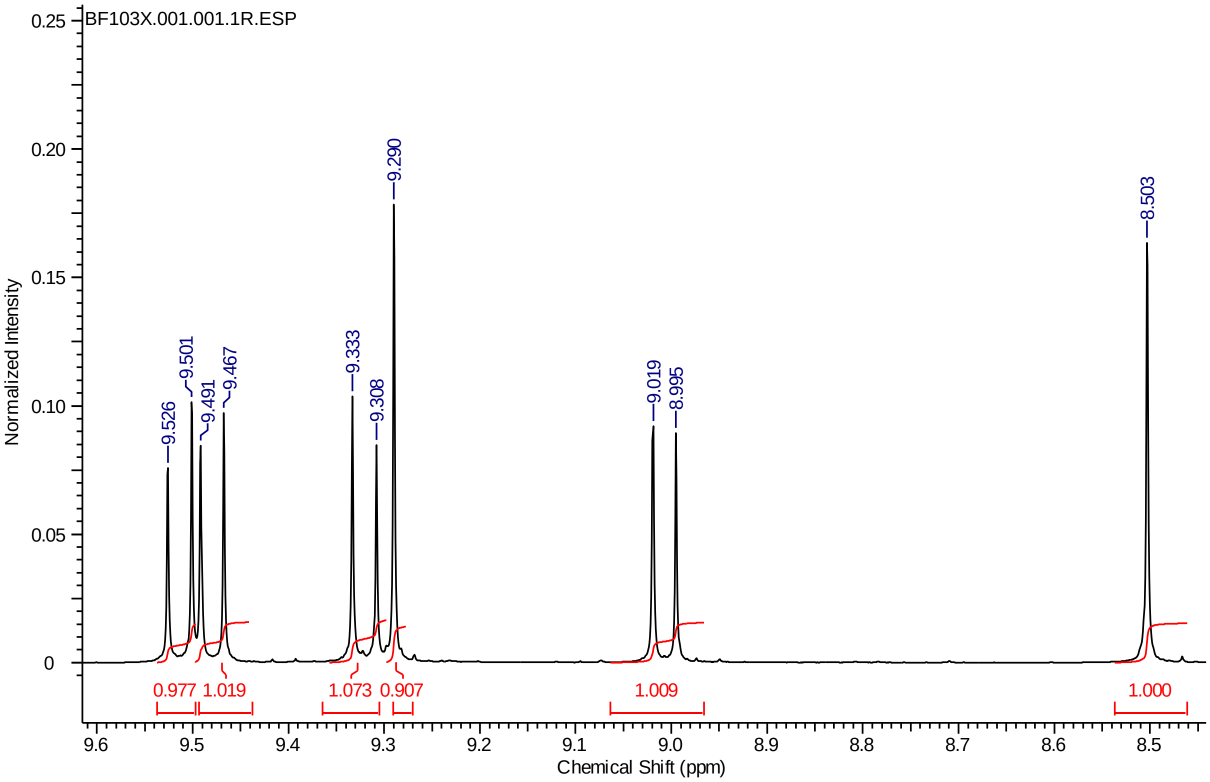

Figure S21: ^{1}H-NMR spectrum of **3c** (zoomed).

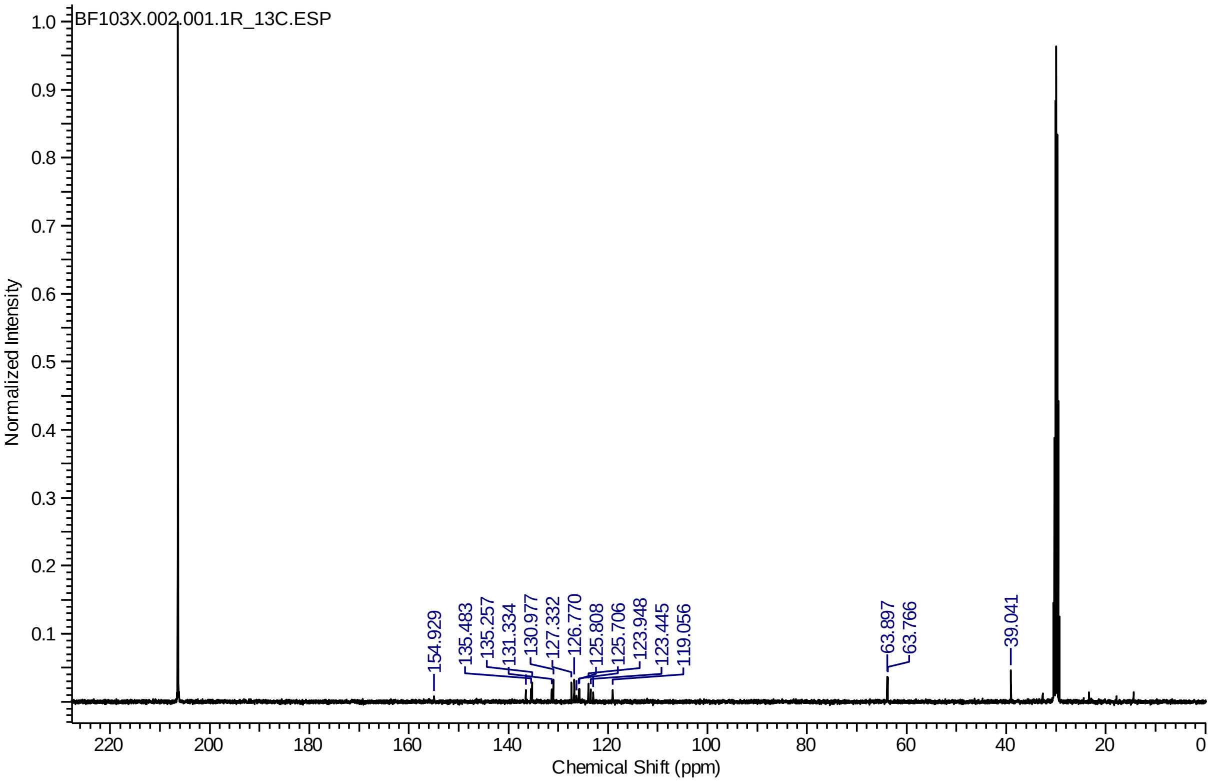

Figure S22: ^{13}C-NMR spectrum of **3c**.

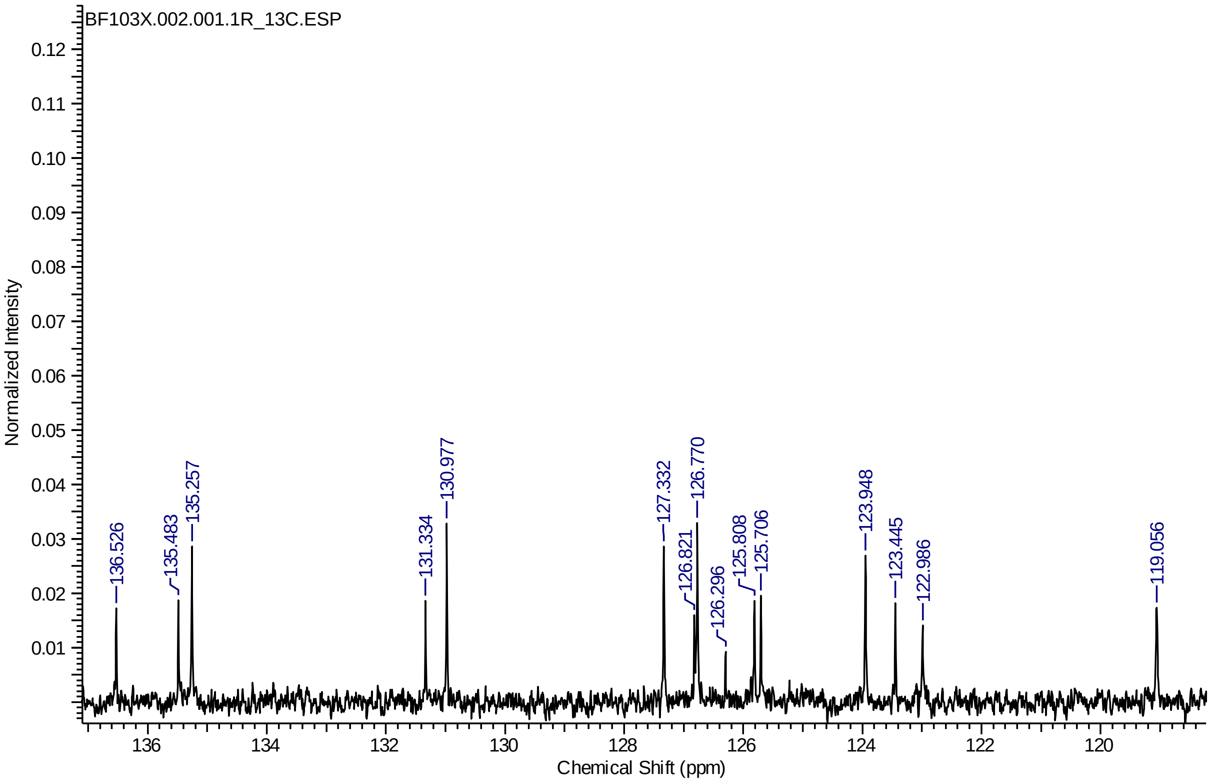

Figure 23: ^{13}C-NMR spectrum of **3c** (zoomed).

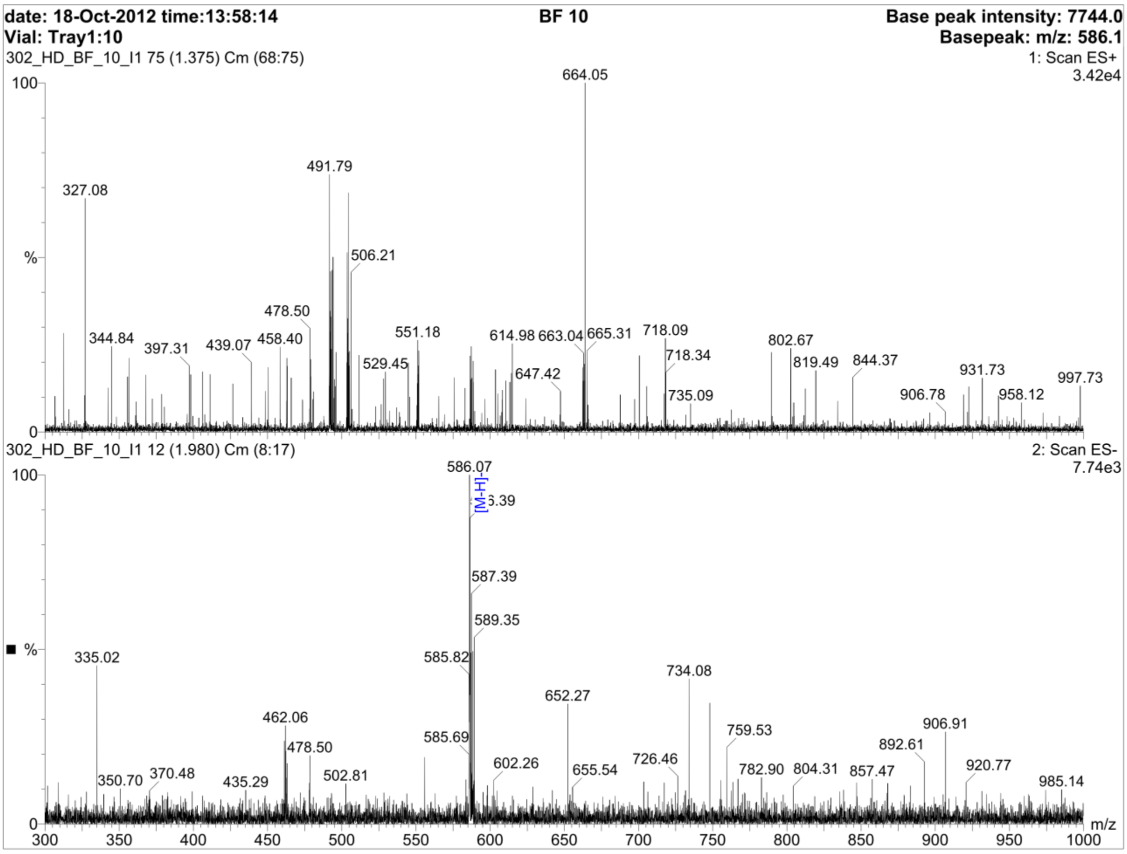

Figure S24: mass spectrum of **3d**.

Compound **3d**:

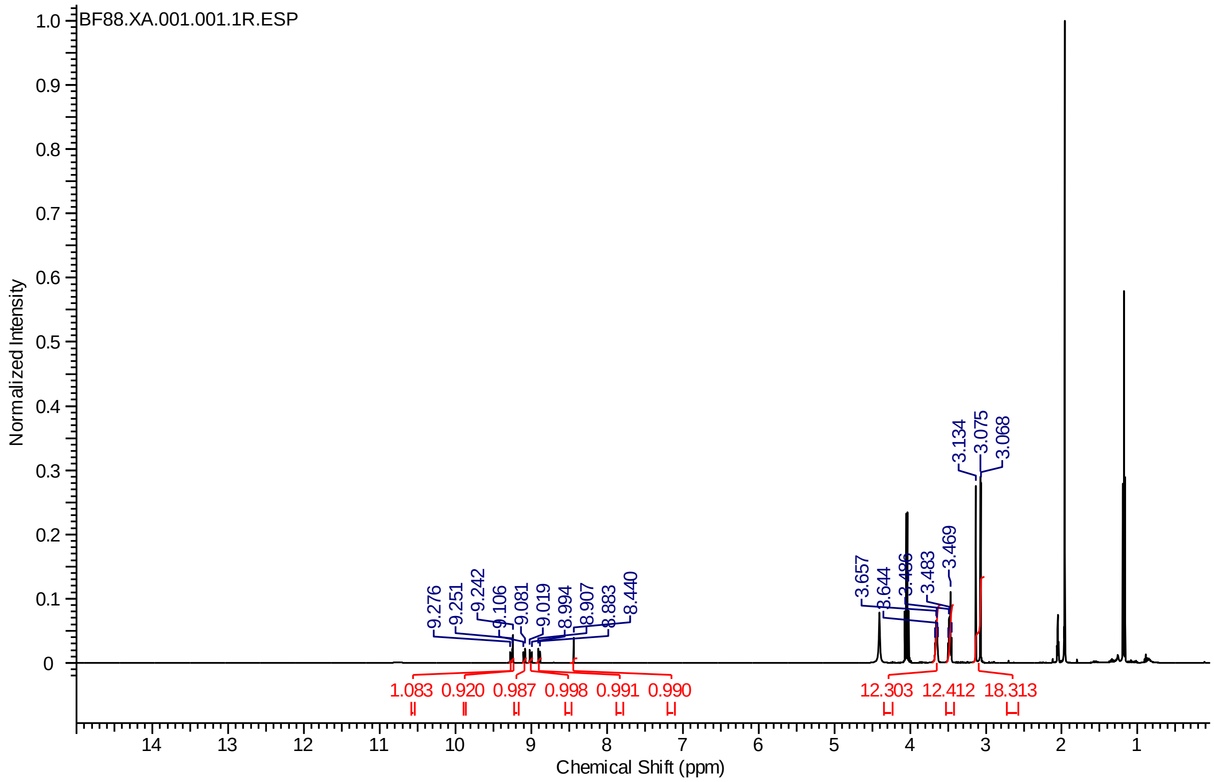

Figure S25: ^{1}H-NMR spectrum of **3d**.

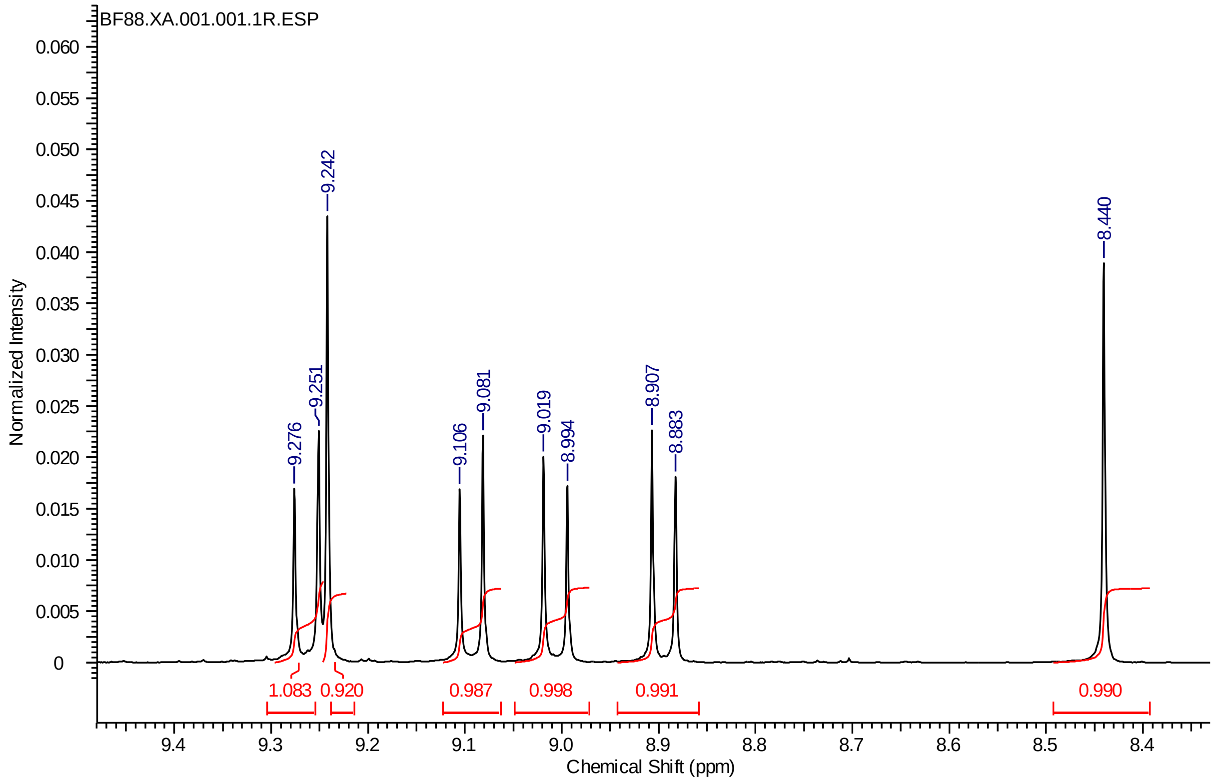

Figure S26: ^{1}H-NMR spectrum of **3d** (zoomed).

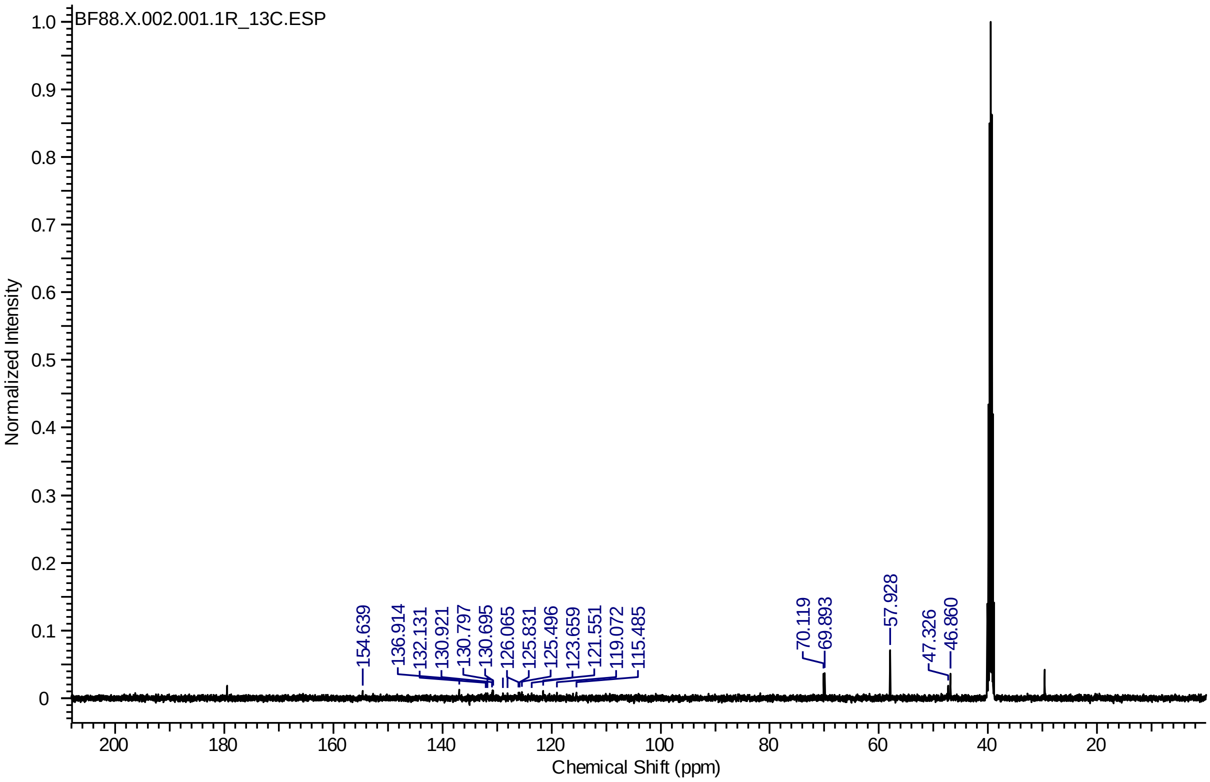

Figure S27: ^{13}C-NMR spectrum of **3d**.

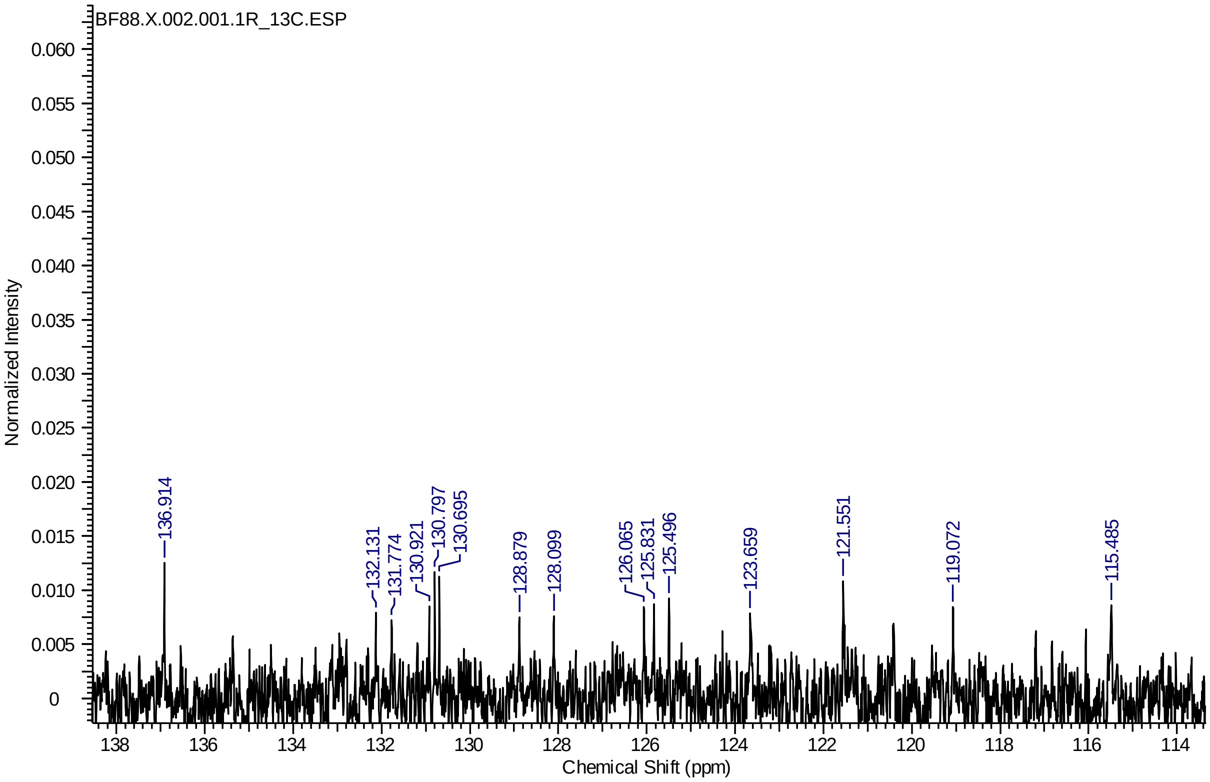

Figure S28: ^{13}C-NMR spectrum of **3d** (zoomed).

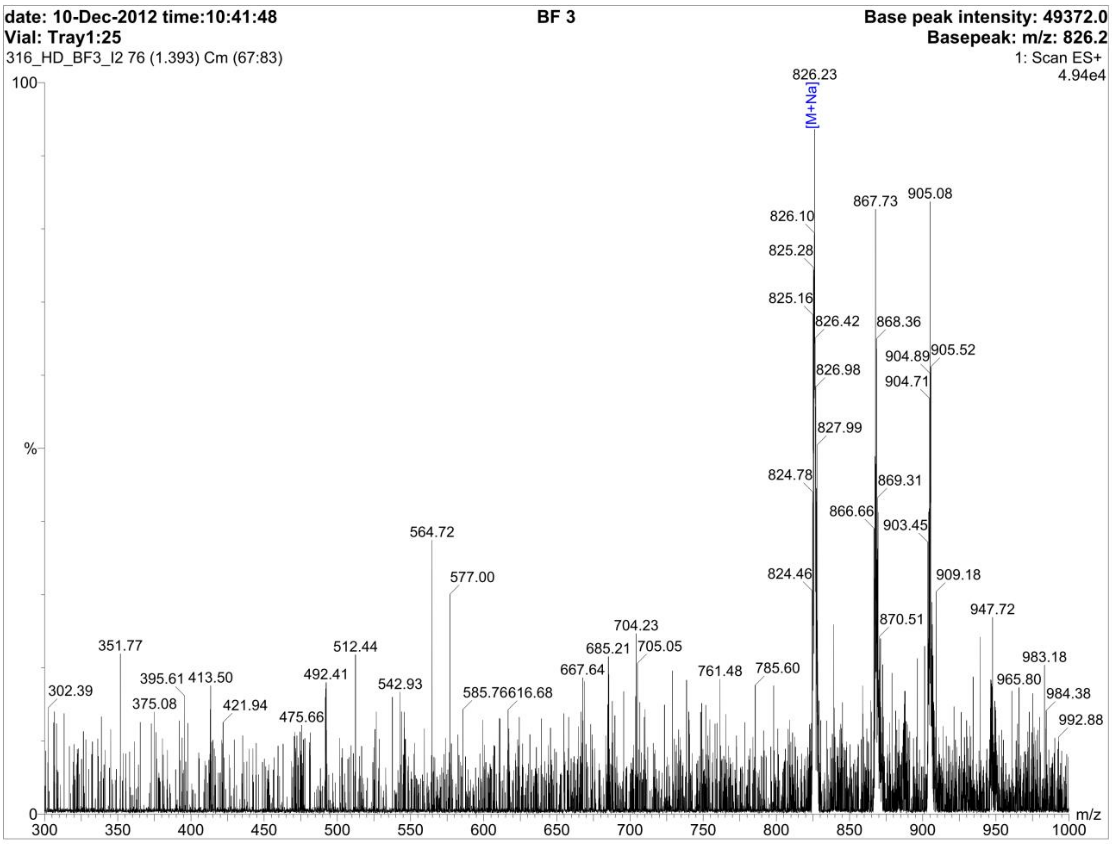

Figure S29: mass spectrum of **3d**.

Compound **3e**:

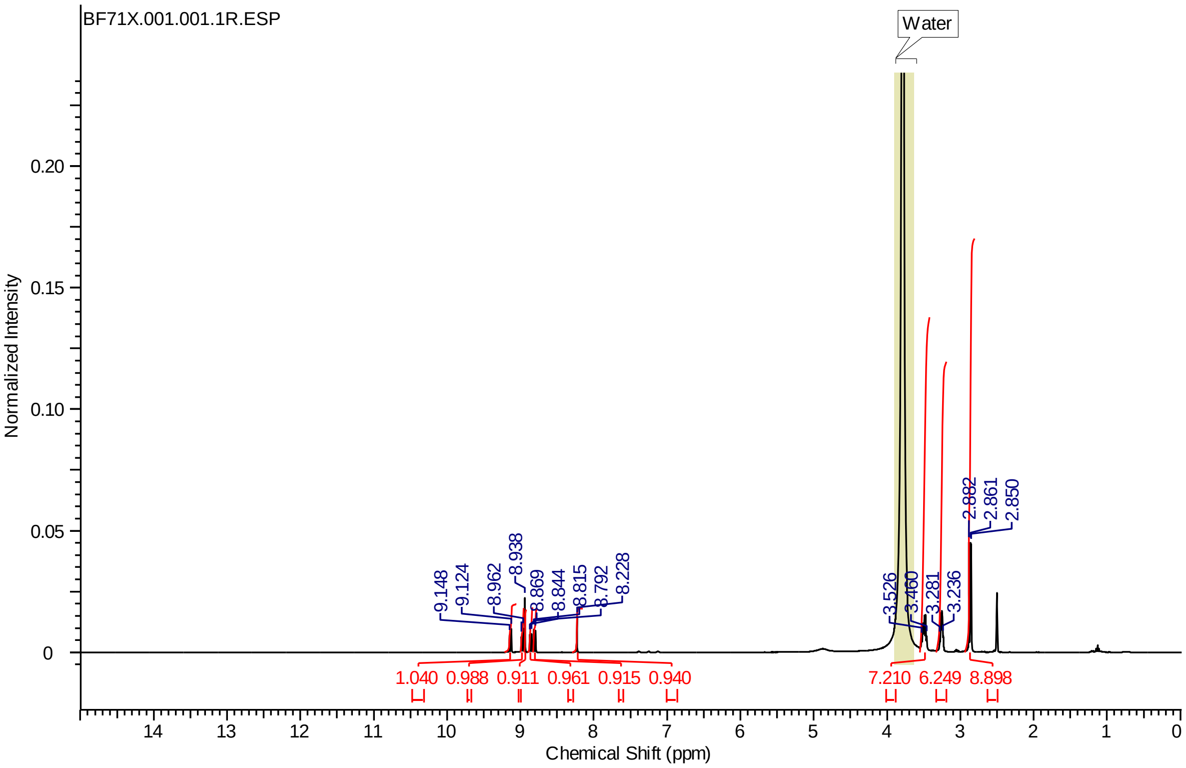

Figure S30: ^{1}H-NMR spectrum of **3e**.

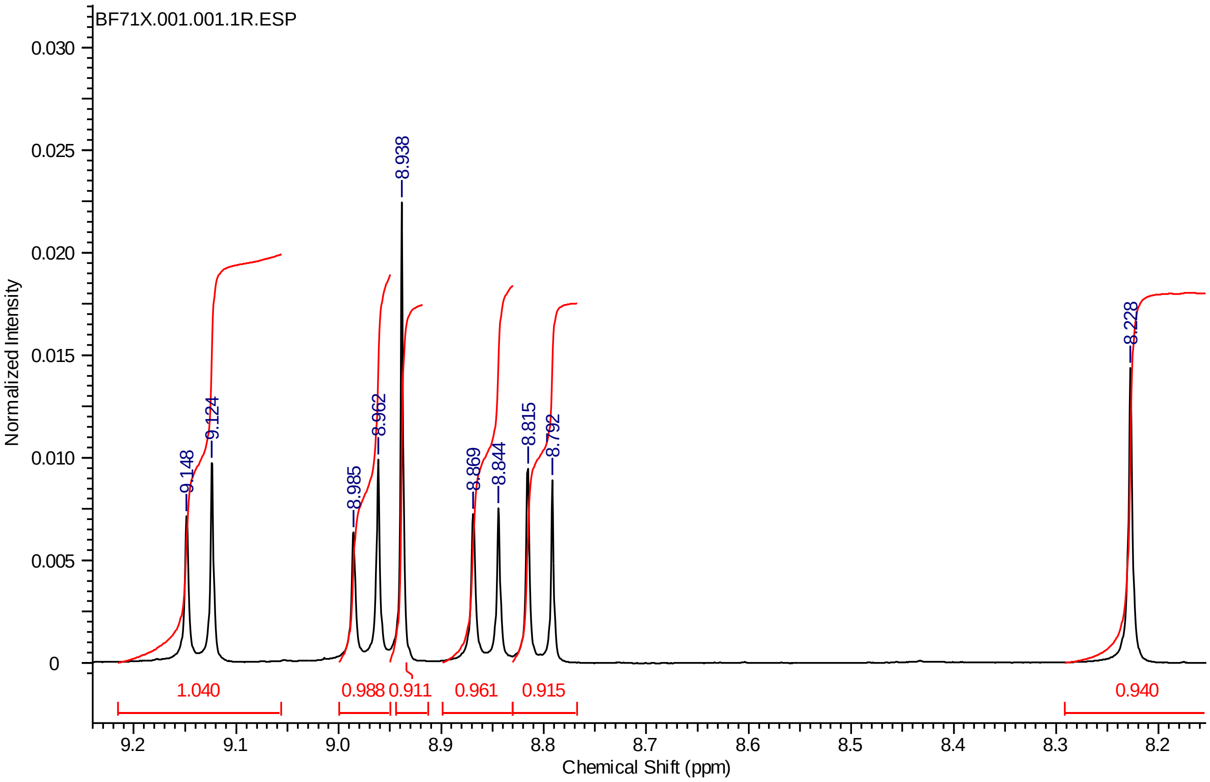

Figure S31: ^{1}H-NMR spectrum of **3e** (zoomed).

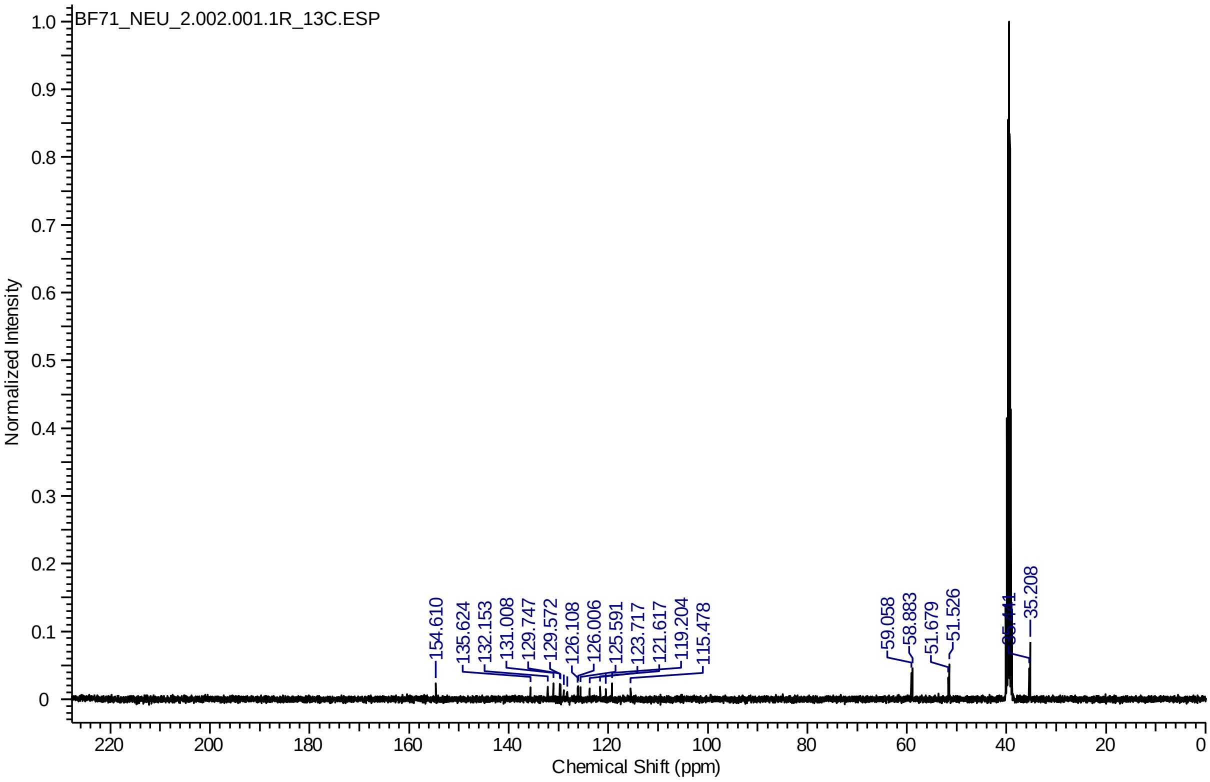

Figure S32: ^{13}C-NMR spectrum of **3e**.

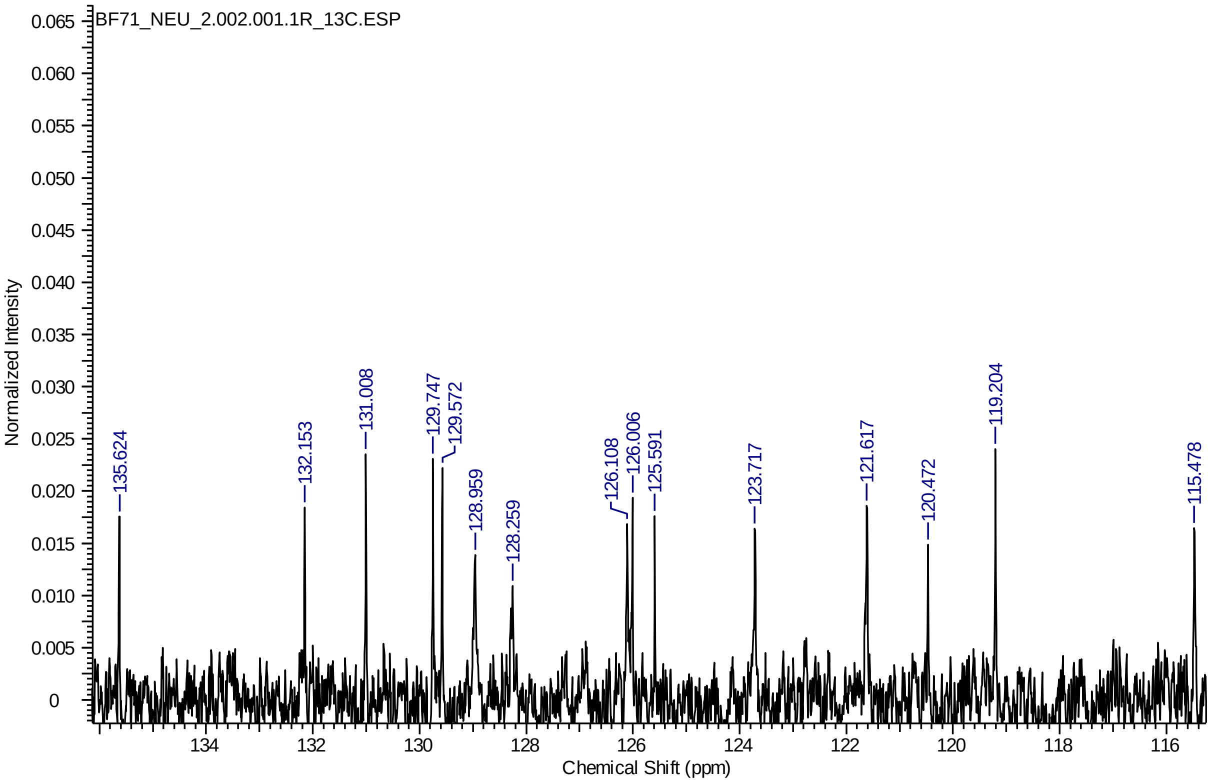

Figure S33: ^{13}C-NMR spectrum of **3e** (zoomed).

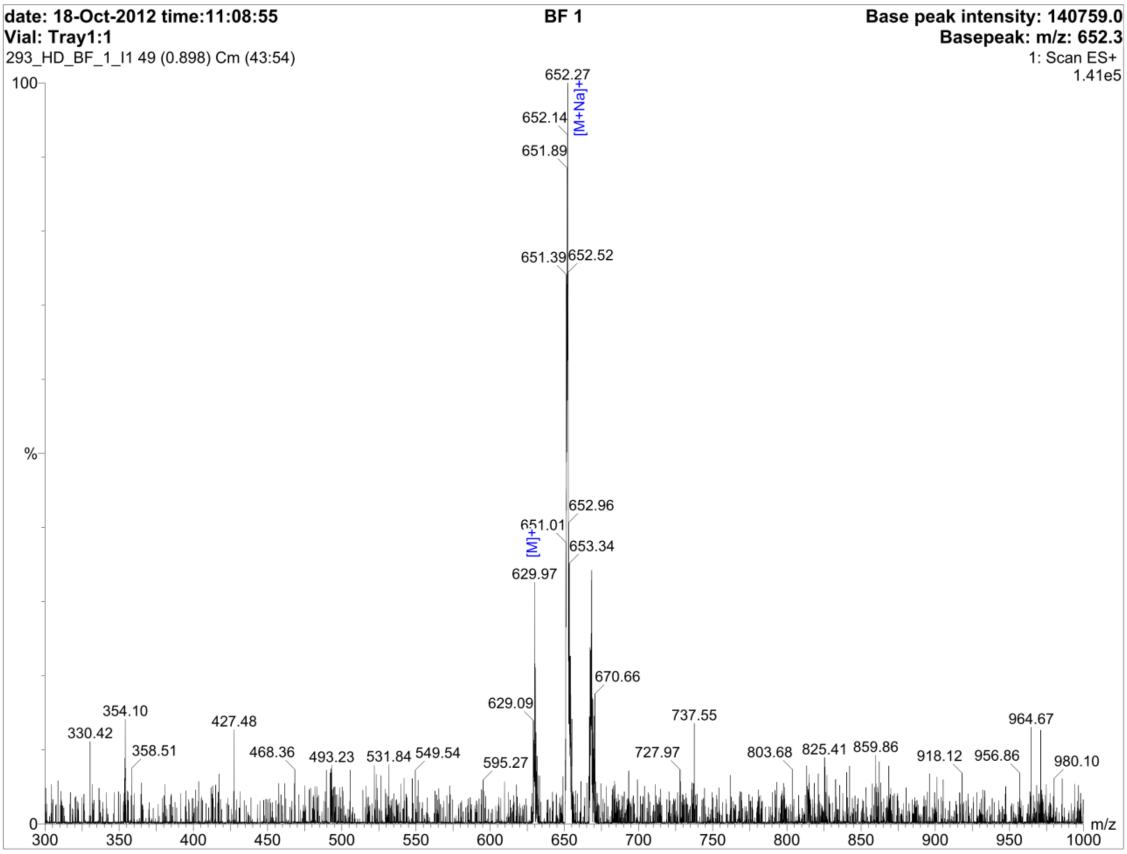

Figure S34: mass spectrum of **3e**.

Compound **3f**:

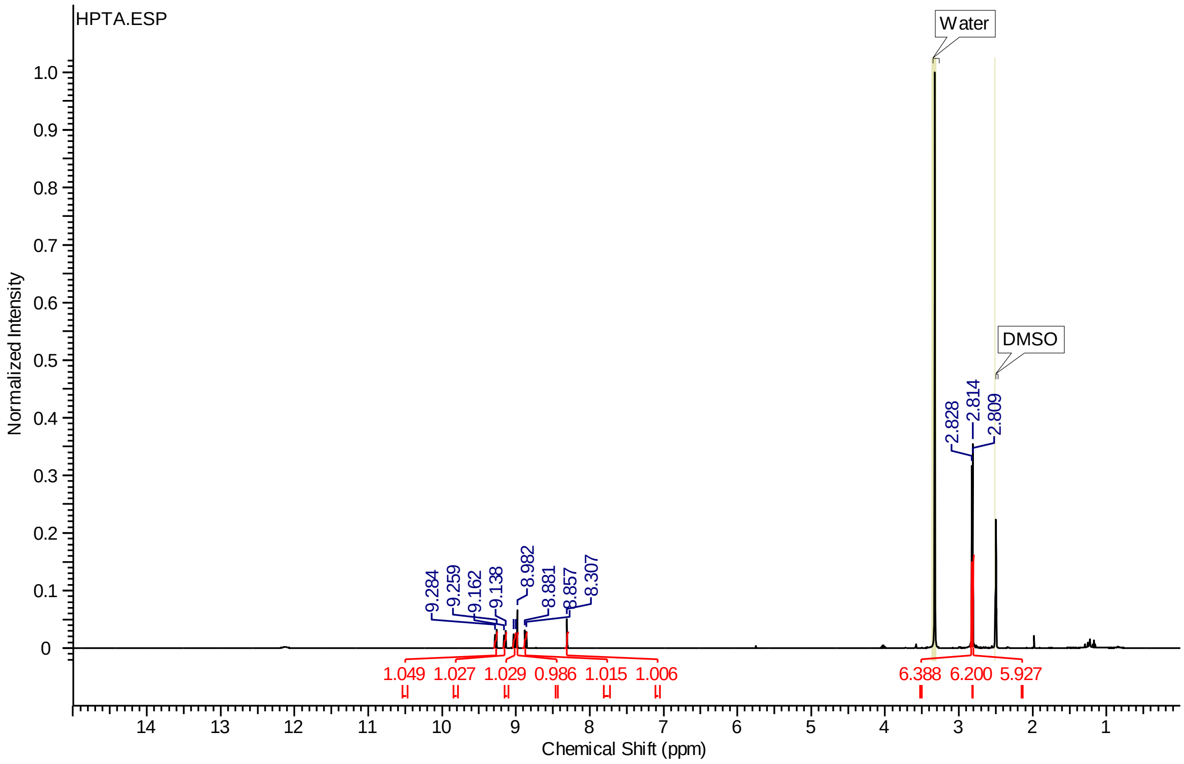

Figure S35: ^{1}H-NMR spectrum of **3f**.

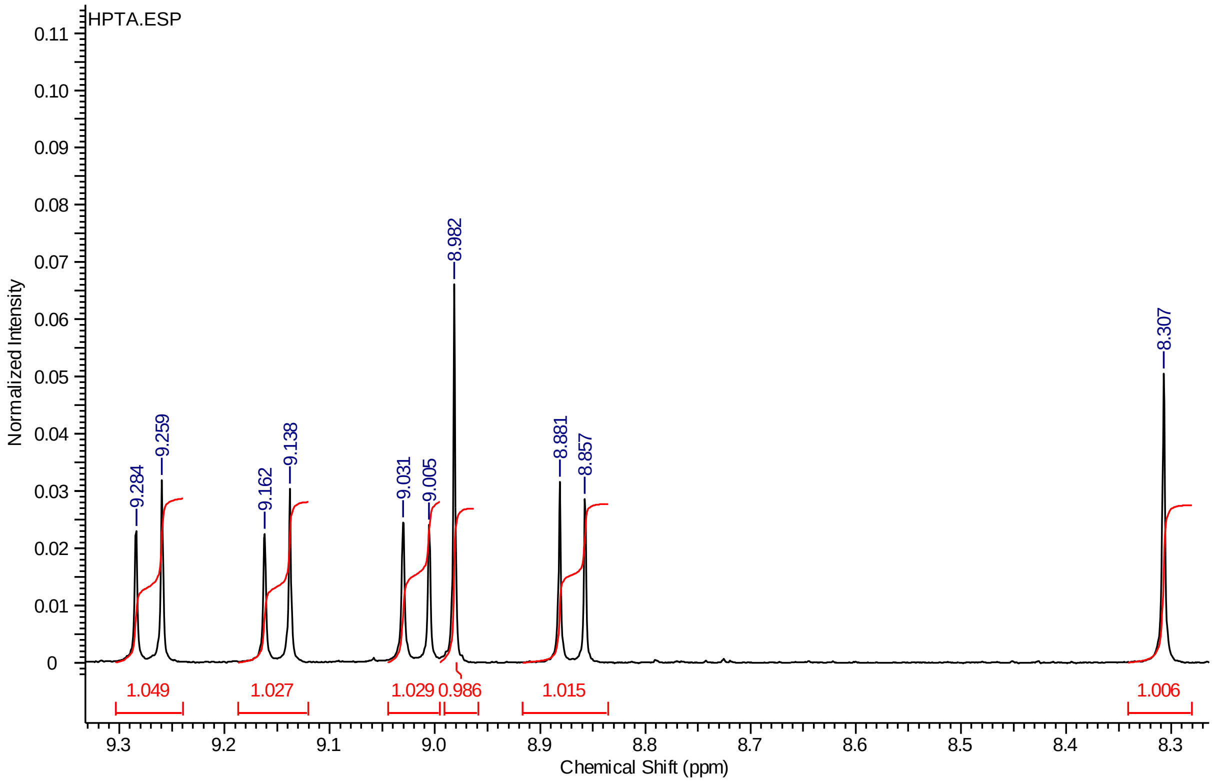

Figure S36: ^{1}H-NMR spectrum of **3f** (zoomed).

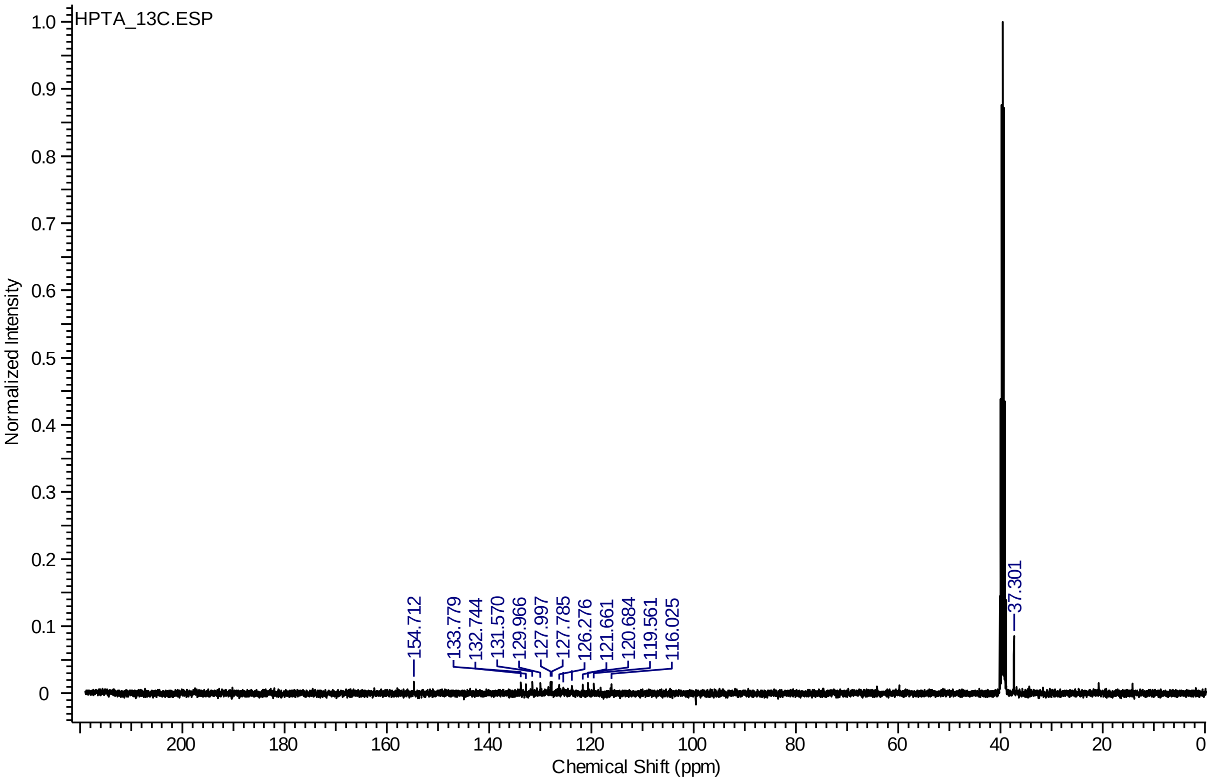

Figure S37: ^{13}C-NMR spectrum of **3f**.

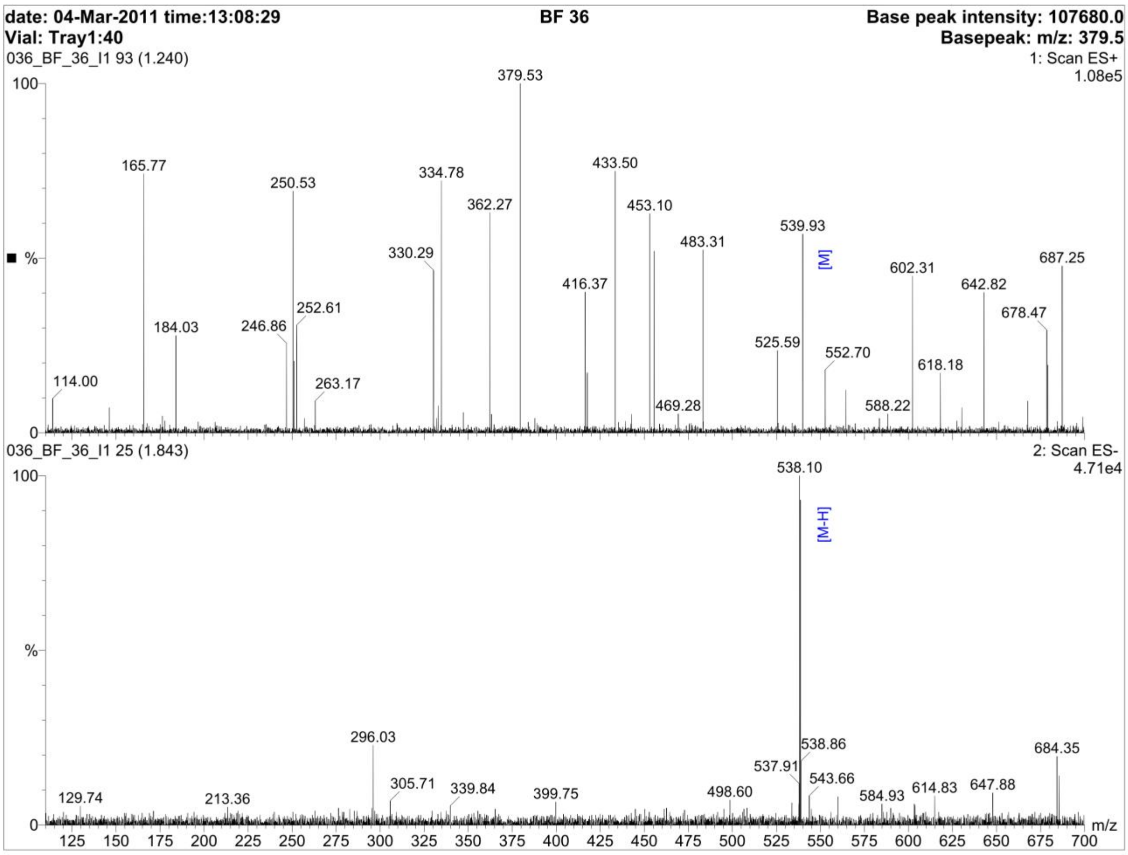

Figure S38: mass spectrum of **3f.**

References:

[S1] J. Widengren, B. Terry, R. Rigler, *Chem. Phys.* **1999**, *249*, 259–271.